

1 **Change in Frozen Soils and the Effects on Regional Hydrology, Upper**  
2 **Heihe Basin, Northeastern Qinghai-Tibetan Plateau**

3 Bing Gao<sup>1</sup>, Dawen Yang<sup>2\*</sup>, Yue Qin<sup>2</sup>, Yuhan Wang<sup>2</sup>, Hongyi Li<sup>3</sup>, Yanlin Zhang<sup>3</sup>, and  
4 Tingjun Zhang<sup>4</sup>

5 <sup>1</sup> School of Water Resources and Environment, China University of Geosciences,  
6 Beijing 100083, China

7 <sup>2</sup> State Key Laboratory of Hydrosience and Engineering, Department of Hydraulic  
8 Engineering, Tsinghua University, Beijing 100084, China

9 <sup>3</sup> Cold and Arid Regions Environmental and Engineering Research Institute, Chinese  
10 Academy of Sciences, Lanzhou, Gansu 730000, China

11 <sup>4</sup> Key Laboratory of West China's Environmental Systems (MOE), College of Earth  
12 and Environmental Sciences, Lanzhou University, Lanzhou, 730000, China

13

14 \* *Corresponding author:* Dawen Yang ([yangdw@tsinghua.edu.cn](mailto:yangdw@tsinghua.edu.cn))

15

16 To be submitted to: The Cryosphere, August 2017

17

18

19 **ABSTRACT:**

20 Frozen ground has an important role in regional hydrological cycles and ecosystems,  
21 especially on the Qinghai-Tibetan Plateau (QTP), which is characterized by high  
22 elevations and a dry climate. This study modified a distributed physically based  
23 hydrological model and applied it to simulate the long-term (from 1971 to 2013)  
24 changes in frozen ground and the effects on hydrology in the upper Heihe basin, which  
25 is located on the northeastern QTP. The model was carefully validated against data  
26 obtained from multiple ground-based observations. Based on the model simulations,  
27 we analyzed the changes in frozen soils and their effects on the hydrology. The results  
28 showed that the permafrost area shrank by 8.8% (approximately 500 km<sup>2</sup>), especially  
29 in areas with elevations between 3500 m and 3900 m. The maximum frozen depth of  
30 seasonally frozen ground decreased at a rate of approximately 0.032 m·decade<sup>-1</sup>, and  
31 the active layer thickness over the permafrost increased by approximately 0.043  
32 m·decade<sup>-1</sup>. Runoff increased significantly during the cold season (November-March)  
33 due to the increase in liquid soil moisture caused by rising soil temperatures. Areas in  
34 which permafrost changed into seasonally frozen ground at high elevations showed  
35 especially large increases in runoff. Annual runoff increased due to increased  
36 precipitation, the base flow increased due to changes in frozen soils, and the actual  
37 evapotranspiration increased significantly due to increased precipitation and soil  
38 warming. The groundwater storage showed an increasing trend, indicating that a  
39 reduction in permafrost extent enhanced the groundwater recharge.

40 **KEYWORDS:** permafrost; seasonally frozen ground; soil moisture; ground

Comment [PDM1]: "particularly"

Comment [PDM2]: "distributed, physically-based"

Comment [PDM3]: "long-term (1971-2013)"

Comment [PDM4]: Delete text

Comment [PDM5]: Delete

Comment [PDM6]: Delete

Comment [PDM7]: "spatio-temporal"

Comment [PDM8]: Delete

Comment [PDM9]: "Our"

Comment [PDM10]: "show"

Comment [PDM11]: "area with"

Comment [PDM12]: Delete

Comment [PDM13]: "predominantly"

Comment [PDM14]: Delete

Comment [PDM15]: "an"

41 temperature; runoff

42 **1. Introduction**

43 Global warming has led to significant changes in frozen soils, including both permafrost  
44 and seasonally frozen ground at high latitudes and high elevations (Hinzman et al., 2013;  
45 Cheng and Wu, 2007). Changes in frozen soils can greatly affect land-atmosphere  
46 interactions and the energy and water balances of the land surface (Subin et al., 2013;  
47 Schuur et al., 2015), altering soil moisture, water flow pathways and stream flow  
48 regimes (Walvoord and Kurylyk, 2016). Understanding the changes in frozen soils and  
49 their impacts on regional hydrology is important for water resources management and  
50 ecosystem protection in cold regions.

51 Previous studies based on either experimental observations or long-term  
52 meteorological or hydrological observations have examined changes in frozen soils and  
53 their impacts on hydrology. Several studies reported that permafrost thawing might  
54 enhance base flow in the Arctic and the Subarctic (Walvoord and Striegl, 2007; Jacques  
55 and Sauchyn, 2009; Ye et al., 2009), as well as in northeastern China (Liu et al., 2003;  
56 Duan et al., 2017). A few studies reported that permafrost thawing might reduce river  
57 runoff (here, runoff is defined as all liquid water flowing out of the study area),  
58 especially on the Qinghai-Tibetan Plateau (e.g., Qiu, 2012; Jin et al., 2009). Intensive  
59 field observations of frozen soils have typically been performed at small spatial scales  
60 over short periods. Consequently, regional patterns and long-term trends have not been  
61 captured. Long-term meteorological and hydrological observations are available, but  
62 they do not provide information on soil freezing and thawing processes (McClelland et  
63 al., 2004; Liu et al., 2003; Niu et al., 2011). Therefore, previous observation-based

Comment [PDM16]: "(QTP)"

Comment [PDM17]: "Those studies that include intensive"

Comment [PDM18]: "(e.g., Cite an example or two)"

Comment [PDM19]: "are not typical"

Comment [PDM20]: "available in many areas"

64 studies have not provided a sufficient understanding of the long-term changes in frozen  
65 soils and their impact on regional hydrology (Woo et al., 2008).

66 Hydrological models have been coupled with soil freezing-thawing schemes to  
67 simulate impacts of the changes in frozen soils on catchment hydrology. Several  
68 hydrological models (Rawlins et al., 2003; Chen et al., 2008) used simple freezing-  
69 thawing schemes, which could not simulate the vertical soil temperature profiles. The  
70 modified VIC model (Cherkauer and Lettenmaier, 1999) and the CLM model (Oleson  
71 et al., 2010) simulate vertical soil freezing-thawing processes, but they simplify the  
72 flow routing using linear schemes. Subin et al. (2013) and Lawrence et al. (2015) used  
73 the CLM model to simulate global changes in permafrost. Cuo et al. (2015) used the  
74 VIC to simulate frozen soil changes and their hydrological impacts at the plot scale in  
75 the headwaters of the Yellow River. The GEOtop model (Endrizzi et al., 2014)  
76 simulates three-dimensional water flux and vertical heat transfer in soil, but it is difficult  
77 to apply for regional investigations. Wang et al. (2010) and Zhang et al. (2013)  
78 incorporated frozen soil schemes in a distributed hydrological model and showed  
79 improved performance in a small mountainous catchment. More regional studies are  
80 necessary to better understand the frozen soil changes and their impacts on regional  
81 hydrologic processes and water resources.

82 The Qinghai-Tibetan Plateau (QTP) is known as Asia's water tower, and runoff  
83 changes on the plateau have significant impacts on water security in downstream  
84 regions (Walter et al., 2010); hence, such changes have attracted considerable attention  
85 in recent years (Cuo et al., 2014). The QTP is characterized by high elevations and a

Comment [PDM21]: "As an alternative strategy, hydrological"

Comment [PDM22]: "but these cannot"

Comment [PDM23]: "to"

Comment [PDM24]: "QTP"

86 cold climate. Consequently, cryospheric processes have great impacts on its  
87 hydrological processes (Cheng and Jin, 2013; Cuo et al., 2014). The thickness of  
88 permafrost on the QTP varies from 1 to 130 m, and the temperature ranges between -  
89 0.5 and -3.5 °C (Yang et al., 2010). Compared with Arctic and Subarctic soils, the  
90 frozen soils on the QTP are more sensitive to increased air temperature (Yang et al.,  
91 2010), and changes in the frozen soils may have more significant impacts on the  
92 regional hydrology.

93 Clear increases in the annual and seasonal air temperatures have been observed on  
94 the QTP (Li et al., 2005; Liu and Chen, 2000; Zhao et al., 2004). Several studies have  
95 shown changes in frozen soils based on long-term observations. For example, Cheng  
96 and Wu (2007) analyzed the soil temperature profiles from boreholes on the QTP and  
97 found that the active layer thickness of frozen soils increased by 0.15-0.50 m during the  
98 period of 1996-2001. Zhao et al. (2004) observed a decreasing trend of freezing depth  
99 in the seasonally frozen soils at 50 stations. Several studies have analyzed the  
100 relationship between changes in frozen soils and river discharge using observational  
101 data (Zhang et al., 2003; Jin et al., 2009; Niu et al., 2011). However, the spatio-temporal  
102 characteristics of the long-term changes in frozen soils are not sufficiently clear. Based  
103 on comprehensive field experiments (Cheng et al., 2014), a hydrological model  
104 coupling cryospheric processes and hydrological processes has been developed (Yang  
105 et al., 2015; Gao et al., 2016). This model provides a solid basis upon which to analyze  
106 the spatio-temporal changes in frozen soils and their impacts on the regional hydrology  
107 in the upper Heihe basin located on the northeastern QTP.

Comment [PDM25]: Delete

Comment [PDM26]: Delete

Comment [PDM27]: Delete

Comment [PDM28]: "basin, "

108 On the basis of previous studies, this study aims to: (1) explore the spatial and  
109 temporal changes in frozen soils using a distributed hydrological model with  
110 comprehensive validation and (2) analyze the hydrological responses to the changes in  
111 frozen soils during the past 40 years in the upper Heihe basin.

Comment [PDM29]: "Specifically". Also, append to the end of the previous paragraph.

## 112 2. Study Area and Data

113 The Heihe River is one of the major inland basins in northwestern China. As shown in  
114 Figure 1, the upper reaches of the Heihe River, representing a drainage area of 10,009  
115 km<sup>2</sup>, are located on the northeastern QTP at elevations of 2200 to 5000 m. The upper  
116 reaches of this river provide the majority of the water supplied to the middle and lower  
117 reaches (Cheng et al., 2014). The annual precipitation in the upper Heihe basin ranges  
118 from 200 to 700 mm, and the mean annual air temperature ranges from -9 to 5 °C.  
119 Permafrost dominates the high elevation region above 3700 m (Wang et al., 2013), and  
120 seasonal frozen ground covers the remaining portion of the study area. Glaciers are  
121 found at elevations above 4000 m, and cover approximately 0.8% of the upper Heihe  
122 basin. The upper Heihe basin contains two tributaries, each with a hydrological station,  
123 i.e., Qilian (on the eastern tributary) and Zhamashike (on the western tributary). The  
124 outlet of the upper Heihe basin also features a hydrological station, namely, Yingluoxia  
125 (see Figure 1).

Comment [PDM30]: "ranging from"

Comment [PDM31]: Delete

Comment [PDM32]: Delete

Comment [PDM33]: ",,"

Comment [PDM34]: "one at"

Comment [PDM35]: "and the other at"

Comment [PDM36]: Delete

126 The spatial data used in this study includes atmospheric forcing data, land surface  
127 data and actual evapotranspiration data based on remote sensing. The atmospheric  
128 forcing data include a 1-km gridded dataset of daily precipitation, air temperature,  
129 sunshine hours, wind speed and relative humidity. The gridded daily precipitation was

130 interpolated from observations at meteorological stations (see Figure 1) provided by the  
131 China Meteorological Administration (CMA) using the method developed by Wang et  
132 al. (2017). The other atmospheric forcing data were interpolated **by** observations at  
133 meteorological stations using the inverse distance weighted method. The interpolation  
134 of air temperature considers the elevation-dependent temperature gradient provided by  
135 the HiWATER experiment (Li et al., 2013).

Comment [PDM37]: "from"

136 The land surface data used to run the model include land use, topography, leaf area  
137 **index**, and soil parameters. The topography data were obtained from the Shuttle Radar  
138 Topography Mission (SRTM) dataset (Jarvis et al., 2008) with a spatial resolution of 90  
139 m. The land use/cover data were provided by the Institute of Botany, Chinese Academy  
140 of Sciences (Zhou and Zheng, 2014). The **leaf area index (LAI)** data with 1-km  
141 resolution were developed by Fan (2014). The soil parameters were developed by Song  
142 et al. (2016) and include the saturated hydraulic conductivity, residual soil moisture  
143 content, saturated soil moisture content, soil sand content, soil clay content and soil  
144 organic content. Monthly actual evapotranspiration data with 1-km resolution during  
145 the period of 2002-2012 were estimated based on remote sensing data (Wu et al., 2012;  
146 Wu, 2013).

Comment [PDM38]: "index (LAI)"

Comment [PDM39]: "LAI"

147 The field observation data used in this study include river discharge, soil  
148 temperature, frozen depth, soil moisture and borehole observations. Daily river  
149 discharge data were obtained from the Hydrology and Water Resources Bureau of  
150 Gansu Province. The CMA provided daily soil temperature data collected at the Qilian  
151 station from January 1, 2004 to December 31, 2013, and daily frozen depth data

152 collected at the Qilian and Yeniugou stations from January 1, 2002 to December 31,  
153 2013. We obtained ground temperature observations from six boreholes, whose location  
154 are shown in Figure 1, from Wang et al. (2013). We used the observations at specific  
155 dates instead of annual averages due to lack of continuous measurement. The borehole  
156 depths are 100 m for T1, 69 m for T2, 50 m for T3, 90 m for T4, and 20 m for T5 and  
157 T7. The HiWATER experiment (Li et al., 2013; Liu et al., 2011) provided the soil  
158 moisture data from January 1 to December 31, 2014 at the A'rou Sunny Slope station  
159 (100.52 E, 38.09 N).

Comment [PDM40]: "a lack of continuous measurements"

### 160 3. Methodology

#### 161 3.1 Brief introduction of the hydrological model

162 This study used the distributed eco-hydrological model GBEHM (geomorphology-  
163 based ecohydrological model), which was developed by Yang et al. (2015) and Gao et  
164 al. (2016). The GBEHM is a spatial distributed model for large-scale river basins. It  
165 employs geomorphologic properties to reduce the lateral two-dimensions into one-  
166 dimension for flow routing within a sub-catchment, which greatly improves the  
167 computational efficiency while retaining the spatial heterogeneity in water flow paths  
168 at the basin scale. As shown in Figure 2, the GBEHM used a 1-km grid system to  
169 discretize the study catchment, and the study catchment was divided into 251 sub-  
170 catchments. A sub-catchment was further divided into flow-intervals along its main  
171 stream. To capture the sub-grid topography, each 1-km grid was represented by a  
172 number of hillslopes with an average length and gradient, but different aspect, which  
173 were estimated from the 90-m DEM. The terrain properties of a hillslope include the

Comment [PDM41]: "which"

Comment [PDM42]: "Each"

**Comment [PDM43]:** Additional hillslope properties include soil and vegetation types"

174 slope length, slope gradient, slope aspect, soil type and vegetation type (Yang et al.,  
175 2015).

176 The hillslope is the basic unit in the hydrological simulation of the water and heat  
177 transfers (both conduction and convection) in the vegetation canopy, snow/glacier, and  
178 soil layers. The canopy interception, radiation transfer in the canopy and the energy  
179 balance of the land surface are described using the methods of SIB2 (Sellers et al., 1985,  
180 1996). The surface runoff on the hillslope is solved using the kinematic wave equation.  
181 The groundwater aquifer is considered as individual storage unit corresponding to each  
182 grid. Exchange between the groundwater and the river water is calculated using Darcy's  
183 law (Yang et al., 1998, 2002; Cong et al., 2009).

184 The model runs with a time step of 1 hour. Runoff generated from the grid is the  
185 lateral inflow into the river over the same flow interval in the corresponding sub-  
186 catchment. Flow routing in the river network is calculated using the kinematic wave  
187 equation following the sequence determined by the Horton-Strahler scheme (Strahler,  
188 1957). The model is driven by the atmosphere forcing data and land surface data  
189 introduced in section 2.

### 190 **3.2 Simulation of cryospheric processes**

191 The simulation of cryospheric processes in the GBEHM includes glacier ablation,  
192 snow melting, and soil freezing and thawing.

#### 193 (1) Glacier ablation

194 Glacier ablation is simulated using the following energy balance model (Oerlemans,  
195 2001):

196 
$$Q_M = SW(1-\alpha) + LW_{in} - LW_{out} - Q_H - Q_L - Q_G + Q_R \quad (1)$$

197 where  $Q_M$  is the net energy absorbed by the surface of the glacier ( $\text{W m}^{-2}$ );  $SW$  is the  
 198 incoming shortwave radiation ( $\text{W m}^{-2}$ );  $\alpha$  is the surface albedo;  $LW_{in}$  is the incoming  
 199 longwave radiation ( $\text{W m}^{-2}$ );  $LW_{out}$  is the outgoing longwave radiation ( $\text{W m}^{-2}$ );  $Q_H$  is  
 200 the sensible heat flux ( $\text{W m}^{-2}$ );  $Q_L$  is the latent heat flux ( $\text{W m}^{-2}$ );  $Q_R$  is the energy from  
 201 rainfall ( $\text{W m}^{-2}$ ); and  $Q_G$  is the penetrating shortwave radiation ( $\text{W m}^{-2}$ ). The surface  
 202 albedo is calculated as follows (Oerlemans and Knap, 1998):

203 
$$\alpha = \alpha_{snow} + (\alpha_{ice} - \alpha_{snow})e^{-h/d^*} \quad (2)$$

204 where  $\alpha_{snow}$  is the albedo of snow on the glacier surface;  $\alpha_{ice}$  is the albedo of the ice  
 205 surface;  $h$  is the snow depth on the glacier surface (m);  $d^*$  is a parameter describing the  
 206 snow depth effect on the albedo (m).

207 The amount of melt water is calculated as (Oerlemans, 2001):

208 
$$M = \frac{Q_M}{L_f} dt \quad (3)$$

209 where  $dt$  is the time step used in the model (s) and  $L_f$  is the latent heat of fusion ( $\text{J kg}^{-1}$ ).

## 211 (2) Snow melt

212 A multi-layer snow cover model is used to describe the mass and energy balance of  
 213 snow cover. The snow parametrization is based on Jordan (1991), and two constituents,  
 214 namely, ice and liquid water, are used to describe each snow layer. For each snow layer,  
 215 temperature is solved using an energy balance approach (Bartelt and Lehner, 2002):

216 
$$C_s \frac{\partial T_s}{\partial t} - L_f \frac{\partial \rho_i \theta_i}{\partial t} = \frac{\partial}{\partial z} (K_s \frac{\partial T}{\partial z}) + \frac{\partial I_R}{\partial z} + Q_R \quad (4)$$

217 where  $C_s$  is the heat capacity of snow ( $\text{J m}^{-3} \text{K}^{-1}$ );  $T_s$  is the temperature of the snow

218 layer (K);  $\rho_i$  is the density of ice ( $\text{kg}\cdot\text{m}^{-3}$ );  $\Theta_i$  is the volumetric ice content;  $K_s$   
 219 is the thermal conductivity of snow ( $\text{W}\cdot\text{m}^{-1}\text{K}^{-1}$ );  $L_f$  is the latent heat of ice fusion ( $\text{J}\cdot\text{kg}^{-1}$ );  
 220  $I_R$  is the radiation transferred into the snow layer ( $\text{W}\cdot\text{m}^{-2}$ ); and  $Q_R$  is the energy  
 221 delivered by rainfall ( $\text{W}\cdot\text{m}^{-2}$ ), which is only considered for the top snow layer. The solar  
 222 radiation transfer in the snow layers and the snow albedo are simulated using the  
 223 SNICAR model, which is solved using the method developed by Toon et al. (1989). Eq.  
 224 (4) is solved using an implicit centered finite difference method, and a Crank-Nicholson  
 225 scheme is employed.

226 The mass balance of the snow layer is described as follows (Bartelt and Lehmin, 2002):

$$227 \quad \frac{\partial \rho_i \theta_i}{\partial t} + M_{iv} + M_{il} = 0 \quad (5)$$

$$228 \quad \frac{\partial \rho_l \theta_l}{\partial t} + \frac{\partial U_l}{\partial z} + M_{lv} - M_{il} = 0 \quad (6)$$

229 where  $\rho_l$  is the density of the liquid water ( $\text{kg}\cdot\text{m}^{-3}$ );  $\theta_l$  is the volumetric liquid water  
 230 content;  $U_l$  is the liquid water flux ( $\text{kg}\cdot\text{m}^{-2}\cdot\text{s}^{-1}$ );  $M_{iv}$  is the mass of ice that changes into  
 231 vapour within a time step ( $\text{kg}\cdot\text{m}^{-3}\cdot\text{s}^{-1}$ );  $M_{il}$  is the mass of ice that changes into liquid  
 232 water within a time step ( $\text{kg}\cdot\text{m}^{-3}\cdot\text{s}^{-1}$ ); and  $M_{lv}$  is the mass of liquid water that changes  
 233 into vapour within a time step ( $\text{kg}\cdot\text{m}^{-3}\cdot\text{s}^{-1}$ ). The liquid water flux of the snow layer is  
 234 calculated as follows (Jordan, 1991):

$$235 \quad U_l = -\frac{k}{\mu_l} \rho_l^2 g \quad (7)$$

236 where  $k$  is the hydraulic permeability ( $\text{m}^2$ ),  $\mu_l$  is dynamic viscosity of water at  $0\text{ }^\circ\text{C}$   
 237 ( $1.787\cdot 10^{-3}\text{ N}\cdot\text{s}\cdot\text{m}^{-2}$ ),  $\rho_l$  is the density of liquid water ( $\text{kg}\cdot\text{m}^{-3}$ ) and  $g$  is gravitational  
 238 acceleration ( $\text{m}\cdot\text{s}^{-2}$ ). The water flux of the bottom snow layer is considered snowmelt  
 239 runoff.

240 (3) Soil freezing and thawing

241 The energy balance of the soil layer is solved as follows (Flerchinger and Saxton,  
242 1989):

$$243 \quad C_s \frac{\partial T}{\partial t} - \rho_i L_f \frac{\partial \theta_i}{\partial t} - \frac{\partial}{\partial z} (\lambda_s \frac{\partial T}{\partial z}) + \rho_l c_l \frac{\partial q_l T}{\partial z} = 0 \quad (8)$$

244 where  $C_s$  is the volumetric soil heat capacity ( $\text{J m}^{-3} \text{K}^{-1}$ );  $T$  is the temperature (K) of  
245 the soil layers;  $z$  is the vertical depth of the soil (m);  $\theta_i$  is the volumetric ice content;  
246  $\rho_i$  is the density of ice ( $\text{kg m}^{-3}$ );  $\lambda_s$  is the thermal conductivity ( $\text{W m}^{-1} \text{K}^{-1}$ );  $\rho_l$  is  
247 the density of liquid water ( $\text{kg m}^{-3}$ ); and  $c_l$  is the specific heat of liquid water  
248 ( $\text{J kg}^{-1} \text{K}^{-1}$ ). In addition,  $q_l$  is the water flux between different soil layers ( $\text{m s}^{-1}$ ) and is  
249 solved using the 1-D vertical Richards equation. The unsaturated soil hydraulic  
250 conductivity is calculated using the modified van Genuchten's equation (Wang et al.,  
251 2010), as follows:

$$252 \quad K = f_{ice} K_{sat} \left( \frac{\theta_l - \theta_r}{\theta_s - \theta_r} \right)^{1/2} \left[ 1 - \left( 1 - \left( \frac{\theta_l - \theta_r}{\theta_s - \theta_r} \right)^{1/m} \right)^m \right]^2 \quad (9)$$

253 where  $K$  is the unsaturated soil hydraulic conductivity ( $\text{m s}^{-1}$ );  $K_{sat}$  is the saturated  
254 soil hydraulic conductivity ( $\text{m s}^{-1}$ );  $\theta_l$  is the volumetric liquid water content;  $\theta_s$  is  
255 the saturated water content;  $\theta_r$  is the residual water content;  $m$  is an empirical  
256 parameter in van Genuchten's equation and  $f_{ice}$  is an empirical hydraulic conductivity  
257 reduction factor that is calculated using soil temperature as follows (Wang et al., 2010):

$$258 \quad f_{ice} = \exp[-10(T_f - T_{soil})], \quad 0.05 \leq f_{ice} \leq 1 \quad (10)$$

259 where  $T_f$  is 273.15 K and  $T_{soil}$  is the soil temperature.

260 Eq. (8) solves the soil temperature with the upper boundary condition as the heat flux  
261 into the uppermost soil layer. When the ground is not covered by snow, the heat flux

Comment [PDM44]: "Equation"

262 from the atmosphere into the uppermost soil layer is expressed as follows (Oleson et  
263 al., 2010):

$$264 \quad h = S_g + L_g - H_g - \lambda E_g + Q_R \quad (11)$$

265 where  $h$  is the upper boundary heat flux into the soil layer ( $\text{W}\cdot\text{m}^{-2}$ );  $S_g$  is the solar  
266 radiation absorbed by the uppermost soil layer ( $\text{W}\cdot\text{m}^{-2}$ );  $L_g$  is the net long wave  
267 radiation absorbed by the ground ( $\text{W}\cdot\text{m}^{-2}$ ),  $H_g$  is the sensible heat flux from the ground  
268 ( $\text{W}\cdot\text{m}^{-2}$ );  $\lambda E_g$  is the latent heat flux from the ground ( $\text{W}\cdot\text{m}^{-2}$ ); and  $Q_R$  is the energy  
269 delivered by rainfall ( $\text{W}\cdot\text{m}^{-2}$ ). When the ground is covered by snow, the heat flux into  
270 the uppermost soil layer is calculated as follows:

$$271 \quad h = I_p + G \quad (12)$$

272 where  $I_p$  is the radiation that penetrates the snow cover, and  $G$  is the heat conduction  
273 from the bottom snow layer to the uppermost soil layer. Eq (8) is solved using a finite  
274 difference scheme with an hourly time step, similar to the solution of Eq (4).

275 There are no available observations of the geothermal heat flux for the northeastern  
276 QTP. To simulate the permafrost we consider an underground depth of 50 m. We assume  
277 an upward thermal heat flux at the bottom boundary and estimate its value to be 0.14  
278  $\text{W}\cdot\text{m}^{-2}$  at a depth of 50 m using the average geothermal gradient from the 4 boreholes  
279 (T1-T4) shown in Figure 3, which is reasonable based on a comparison with the  
280 observations ( $0.02\text{ W}\cdot\text{m}^{-2}$  to  $0.16\text{ W}\cdot\text{m}^{-2}$ ) from the interior of the QTP (Wu et al., 2010).

281 The vertical soil column is divided into 39 layers in the model (see Figure 2). The 1.7  
282 m topsoil layer is subdivided into 9 layers. The first layer is 0.05 m, and the soil layer  
283 thickness increases with depth linearly from 0.05 m to 0.3 m at a depth of 0.8 m and

Comment [PDM45]: "simulate permafrost we"

Comment [PDM46]: "soil "

Comment [PDM47]: "at the surface"

Comment [PDM48]: delete

Comment [PDM49]: "thicknesses increase"

284 then decreases linearly with depth to 0.1 m at a depth of 1.7 m. There are 12 soil layers  
285 with a constant thickness of 0.1 m from 1.7 m to 3.0 m to try to replicate the maximum  
286 freezing depths according to field observations. From the depth of 3 m to 50 m, there  
287 are 18 layers with thicknesses increasing exponentially from 0.1 m to 12 m. The liquid  
288 soil moisture, ice content, and soil temperature of each layer is calculated at each time  
289 step. The soil heat capacity and soil thermal conductivity are estimated using the  
290 method developed by Farouki (1981).

### 291 3.3 Model calibration

292 To initialize the model, we first estimated the soil temperature profiles based on the  
293 assumption that there is a linear relationship between the ground temperature at a given  
294 depth below the surface and elevation. This temperature-elevation relationship is  
295 estimated from the observed ground temperatures in 6 boreholes (see Figure 1). Next,  
296 the model had a 500-year spin up run to specify the initial values of the hydrological  
297 variables (e.g., soil moisture, soil ice content, ground temperature, and groundwater  
298 table) by repeating the atmospheric forcing data from 1961 to 1970.

299 This study used the period of 2002 to 2006 for model calibration and the period of  
300 2008 to 2012 for model validation. The daily ground temperature at the Qilian station  
301 and the frozen depths at the Qilian and Yeniugou stations were used to calibrate the  
302 ground surface reflectance according to vegetation type. The other parameters, such as  
303 groundwater hydraulic conductivity, were calibrated according to the observed  
304 baseflow discharge in the winter season at the Qilian, Zhamashike and Yingluoxia  
305 stations. We calibrated the surface retention capacity and surface roughness to match

Comment [PDM50]: "m. Then thicknesses decrease linearly with depth reaching"

Comment [PDM51]: "From 1.7 m to 3.0 m depth, there"

Comment [PDM52]: "to try to capture"

306 the observed flood peaks, and calibrated the leaf reflectance, leaf transmittance and  
307 maximum Rubisco capacity of the top leaf based on the remote sensing  
308 evapotranspiration data. Table 1 shows the major parameters used in the model.

309 We also simulated the hydrological processes without the frozen soil scheme to  
310 investigate the impact of frozen soils. In this case, the phase transition of soil water  
311 between the solid and the liquid is not considered, although the ground temperature is  
312 still simulated. Other processes are simulated in the same manner as in the normal run.

## 313 **4. Results**

### 314 **4.1 Validation of the hydrological model**

315 We conducted a comprehensive validation of the GBEHM using the ground  
316 temperature profiles observed from six boreholes, the long-term observations of ground  
317 temperature and frozen depths from the Qilian and Zhamashike stations, the soil  
318 moisture observations from the A'rou Sunny Slope station, the long-term observations  
319 of streamflow from the three hydrological stations shown in Figure 1 and the monthly  
320 actual evapotranspiration estimated from remote sensing data.

321 Figure 3 shows the comparison of the model-simulated and observed ground  
322 temperature profiles at the six boreholes. The model generally captured the vertical  
323 distribution of the ground temperature at T1, T2, T3 and T4 in the permafrost area, but  
324 the temperatures were overestimated above 20 m depth for T1 and T3. Good agreement  
325 between the simulated and observed ground temperature profiles below the depth of 20  
326 m is probably due to fitting of initial values. Therefore, the deep ground temperatures  
327 are stable, which is confirmed by the comparison of temperature profiles in different

Comment [PDM53]: "in order to"

328 years, as shown in Figure S1 in the supplementary material. Figure S1 also illustrates  
329 that the temperatures above 20 m have shown significant increasing trends over the past  
330 40 years. The errors in simulating the vertical temperature profile near the surface might  
331 be caused by simplification of the 3-D topography. At T5, which is located in seasonally  
332 frozen ground, the simulated ground temperature profile did not agree well with the  
333 observed profile at depths of 4-20 m. This error might also be related to heterogeneity  
334 in the ground properties, especially the thermal conductivity and heat capacity, since no  
335 such information was available. The model simulation agrees well with the borehole  
336 observations at T7, which is located in the transition zone from permafrost to seasonally  
337 frozen ground. Therefore, the model can identify the boundary between the permafrost  
338 and seasonally frozen ground.

339 We also validated the model simulation of the freezing/thawing cycles based on long-  
340 term observations of ground temperature and frozen depth. Figure 4 compares the  
341 simulated ground temperature with the observed temperature at the Qilian station,  
342 which is located in seasonally frozen ground (observed daily ground temperature data  
343 are available from 2004). Generally, the model simulations accurately captured the  
344 seasonal changes in the ground temperature profile. Validation of the ground  
345 temperature at different depths (0.05 m, 0.1 m, 0.2 m, 0.4 m, 0.8 m, 0.16 m, and 0.32  
346 m) showed that the root mean square error (RMSE) decreases with increasing depth.  
347 The RMSE was approximately 2.5 °C for the uppermost three depths (0.5 m, 0.10 m  
348 and 0.2 m). The RMSE for depths of 0.4 cm and 0.8 m were 1.7 °C and 1.5 °C,  
349 respectively, and the RMSE for a depth of 3.2 m was 0.9 °C. Uncertainties in the

350 simulations may be related to the ground heat capacity and thermal conductivity  
351 estimated according to Farouki (1981), and the results are similar to the findings by Ou  
352 et al. (2016) using the Northern Ecosystem Soil Temperature (NEST) model. We  
353 compared the model-simulated daily frozen depth with in situ observations at the Qilian  
354 and Yeniugou stations from 2002 to 2014, as shown in Figure 5. The model reproduced  
355 well the daily variations in frozen depth, although the depth was underestimated by  
356 approximately 0.5 m at the Yeniugou station. In general, the validation of ground  
357 temperature and frozen depth indicates that the model effectively captured the freezing  
358 and thawing processes in the upper Heihe basin.

359 Furthermore, we used the the observed hourly liquid soil moisture at the A'rou Sunny  
360 Slope station for an additional independent validation. Figure S2 in the supplementary  
361 material shows the comparison between the simulated and observed liquid soil moisture  
362 at different depths from January 1 to December 31, 2014. This comparison  
363 demonstrates that the model simulation of liquid soil moisture is reasonable.

364 Figure 6 compares the model simulated and the observed daily streamflow discharge  
365 at the Yingluoxia, Qilian and Zhamashike stations. The model simulations agreed well  
366 with the observations. The model simulations captured the flood peaks and the  
367 magnitude of base flow in both the calibration and validation periods. For the  
368 Yingluoxia, Qilian and Zhamashike stations, the Nash-Sutcliffe efficiency (NSE)  
369 coefficients were 0.64, 0.63 and 0.72, respectively, in the calibration period and 0.64,  
370 0.60, and 0.73, respectively, in the validation period. The relative error (RE) was within  
371 10% for both the calibration and validation periods (see Figure 6). Figure S3 in the

Comment [PDM54]: "depth,"

Comment [PDM55]: Line is needed in methods section to describe how simulated versus observed discharge are compared or assessed.

Comment [PDM56]: Delete

372 supplementary material shows the comparison of the model-simulated monthly actual  
373 evaporation data and the remote sensing-based evaporation data for the entire  
374 calibration and validation periods. The GBEHM simulation showed similar temporal  
375 variations in actual evapotranspiration compared with the remote sensing based  
376 estimation, and the RMSE of the simulated monthly evapotranspiration was 9.1 mm in  
377 the calibration period and 7.1 mm in the validation period.

378 We also compared the model-simulated river discharges with and without the frozen  
379 soil scheme. Table S1 in the supplementary material shows that the model with the  
380 frozen soil scheme achieves a better simulation of the daily hydrograph than the model  
381 without the frozen soil scheme. Figure S4 in the supplementary material shows that the  
382 model without the frozen soil scheme overestimates the river discharge in the freezing  
383 season and underestimates flood peaks in the warming season.

#### 384 **4.2 Long-term changes in frozen soils**

385 In the upper Heihe basin, the ground surface starts to freeze in November and begins  
386 to thaw in April (Wang et al., 2015a). From November to March, the ground surface  
387 temperature is below 0°C in both the permafrost and seasonally frozen ground regions,  
388 and precipitation mainly falls in the period from April to October. Therefore, to  
389 investigate the changes in frozen soils and their hydrological impact, a year is  
390 subdivided into two seasons, i.e., the freezing season (November to March) and the  
391 thawing season (April to October). Increasing precipitation and air temperature in the  
392 study area in both seasons over the past 50 years were reported in a previous study  
393 (Wang et al., 2015b). Compared to the decadal mean for 1971 to 1980, the annual mean

394 air temperature for the 2001 to 2010 period was approximately 1.2 °C higher, with a  
395 larger increase in the freezing season (1.4 °C) than in the thawing season (1.1 °C)  
396 (Table S2).

397 Figure 7 shows the changes in the basin-averaged ground temperature in the freezing  
398 and thawing seasons. The ground temperature increased in all seasons, especially over  
399 the past 30 years. The increasing trend of ground temperature was larger in the freezing  
400 season than in the thawing season. In the freezing season (Figure 7(a)), the top layer  
401 ground temperature was lower than the deep layer temperature. The linear trend of the  
402 top layer (0-0.5 m) ground temperature was 0.49 °C ·decade<sup>-1</sup> and the trend of the deep  
403 layer (2.5-3 m) temperature was 0.32 °C ·decade<sup>-1</sup>. The ground temperature in the deep  
404 layer (2.5-3 m) changed from -0.7 °C in the 1970s to approximately 0 °C in the most  
405 recent decade. In the thawing season (Figure 7(b)), the increasing trend of the top layer  
406 (0-0.5 m) ground temperature (0.29 °C ·decade<sup>-1</sup>) was greater than that of the deep layer  
407 (2.5-3 m) temperature (0.22 °C ·decade<sup>-1</sup>). The warming trend was larger in shallow  
408 ground layers; this is because the surface heat flux is impeded by the thermal inertia as  
409 it penetrates to greater depths.

410 Permafrost is defined as ground with a temperature at or below 0 °C for at least two  
411 consecutive years (Woo, 2012). This study differentiated permafrost from seasonally  
412 frozen ground based on the simulated vertical ground temperature profile in each grid.  
413 For each year in each grid, the frozen ground condition was determined by searching  
414 the ground temperature profile within a four-year window from the previous three years  
415 to the current year. Figure 8 shows the change in permafrost area during 1971-2013. As

**Comment [PDM57]:** This text should be moved to Methods.

416 shown in Figure 8(a), the permafrost areas decreased by approximately 8.8% (from  
417 5700 km<sup>2</sup> in the 1970s to 5200 km<sup>2</sup> in the 2000s), indicating an evident decrease in the  
418 permafrost extent in the upper Heihe basin in the past 40 years.

419 Figure 8 (b) shows the changes in the basin-averaged maximum frozen depth in the  
420 seasonally frozen ground areas and active layer thickness in the permafrost areas. The  
421 basin-averaged annual maximum frozen depth showed a significant decreasing trend  
422 (0.032 m-decade<sup>-1</sup>). In addition, the maximum frozen depth had a significantly negative  
423 correlation with the annual mean air temperature ( $r = -0.71$ ). Simulated active layer  
424 thickness in the permafrost regions increased (0.043 m-decade<sup>-1</sup>), and correlated  
425 positively with the annual mean air temperature ( $p = 0.005$ ).

426 Figure 9 shows the frozen soil distributions in the periods of 1971 to 1980 and 2001  
427 to 2010. Comparing the frozen soil distributions of the two periods, we observed major  
428 changes in the frozen soils on sunny slopes at elevations between 3500 and 3900 m,  
429 especially in the west tributary, where large areas of permafrost changed into seasonally  
430 frozen ground. Figure S5, illustrating the taliks simulated in the period of 2001-2010,  
431 shows that the taliks were mainly located on the edge of the permafrost area and the  
432 development of taliks was not significant.

433 Figure 10 shows the monthly mean ground temperatures for areas with elevations  
434 between 3300 and 3500 m and over areas with elevations between 3500 and 3700 m in  
435 the upper Heihe basin. In the areas with elevations between 3300 and 3500 m located  
436 in the seasonally frozen ground region, as shown in Figure 10(a), the frozen depth  
437 decreased, and the ground temperature in the deep layer (with depths greater than 2 m)

Comment [PDM58]: Delete

Comment [PDM59]: "that talik development"

Comment [PDM60]: "(Figure 10(a))"

Comment [PDM61]: "decreased and the ground temperature in deep layers (depths..."

438 increased. Figure 10(b) shows that the increase in ground temperature was larger in the  
439 area with higher elevation (3500-3700 m). This figure shows that the thickness of the  
440 permafrost layer decreased as the ground temperature increased, and the permafrost  
441 changed into seasonally frozen ground after 2000. The thaw depths changed slowly  
442 compared with the frozen depths as shown in Figure 10, which may be primarily due  
443 to the geothermal heat flux. Additionally, the faster increase in the air temperature in  
444 the freezing season ( $0.41\text{ }^{\circ}\text{C decade}^{-1}$ ) than in the thawing season ( $0.26\text{ }^{\circ}\text{C decade}^{-1}$ )  
445 may be another reason.

Comment [PDM62]: "surface "

Comment [PDM63]: "depth to the base of permafrost"

#### 446 **4.3 Changes in the water balance and runoff**

447 Table 2 shows the decadal changes in the annual water balance from 1971 to 2010  
448 based on the model simulation. The annual precipitation, annual runoff and annual  
449 runoff ratio exhibited the same decadal variation; however the annual  
450 evapotranspiration maintained an increasing trend starting in the 1970s that was  
451 consistent with the rising air temperature and soil warming. Although the actual  
452 evapotranspiration increased, the runoff ratio remained stable during the past 4 decades  
453 because of the increased precipitation.

454 Figure 11 and Table 2 show the changes in runoff (both simulated and observed) in  
455 different seasons. The model-simulated and observed runoff both exhibited significant  
456 increasing trends in the freezing season and in the thawing season. Therefore, the model  
457 simulation effectively reproduced the observed long-term changes. In the freezing  
458 season, since there was no glacier or snow melting (see Table 2), the runoff was mainly  
459 the subsurface flow (groundwater flow and lateral flow from the unsaturated zone). In

Comment [PDM64]: Delete

460 the thawing season, as shown in Table 2, snowmelt runoff contributed approximately  
461 14% of the total runoff, whereas glacier runoff contributed only a small fraction of the  
462 total runoff (approximately 2.2%). Rainfall runoff was the major component of the total  
463 runoff in the thawing season, and the runoff increase in the thawing season was mainly  
464 due to increased precipitation and snowmelt. As shown in Figure 11, the actual  
465 evapotranspiration increased significantly in both seasons due to increased precipitation  
466 and ground warming. The increasing trend of the actual evapotranspiration was greater  
467 in the thawing season than in the freezing season.

Comment [PDM65]: "increase in

468 Figure 12 shows the changes in the basin-averaged annual water storage in the top  
469 0-3 m layer and the groundwater storage. The annual liquid water storage of the top 0-  
470 3 m showed a significant increasing trend, especially in the most recent 3 decades. This  
471 long-term change in liquid water storage was similar to the runoff change in the freezing  
472 season, as shown in Figure 11 (a), exhibiting a correlation coefficient of 0.79. The  
473 annual ice water storage in the top 0-3 m soil layers showed a significant decreasing  
474 trend due to frozen soil changes. Annual groundwater storage showed a significantly  
475 increasing trend especially in the most recent 3 decades, which indicates that the  
476 groundwater recharge has increased with the frozen soil degradation.

Comment [PDM66]: "liquid soil "

Comment [PDM67]: (0-3 m)

Comment [PDM68]: Delete

Comment [PDM69]: "soil "

Comment [PDM70]: Delete

Comment [PDM71]: "permafrost"

## 477 5. Discussion

### 478 5.1 Impact of frozen soil changes on the soil moisture and runoff

479 We have plotted the long-term changes in the spatially averaged liquid soil moistures  
480 in the areas with elevations between 3300 and 3500 m and in the areas with elevations  
481 between 3500 and 3700 m in Figure S6 in the supplementary material. In the seasonally

482 frozen ground at elevations of 3300-3500 m, the liquid soil moisture increased slightly  
483 due to the decrease in the frozen depth, as shown in Figure 10(a). At elevations of 3500-  
484 3700 m, the liquid soil moisture in the deep layer increased significantly since the 1990s,  
485 due to the change of the permafrost into seasonally frozen ground, as shown in Figure  
486 10 (b).

Comment [PDM72]: " (Figure 10(a))

Comment [PDM73]: " (Figure 10(b))

487 In the freezing season, since the surface ground is frozen, runoff is mainly subsurface  
488 flow coming from the seasonally frozen ground. Runoff has the highest correlation ( $r =$   
489 0.82) with the liquid soil moisture in the freezing season, which indicates that the frozen  
490 soil changes were the primary cause of the increased liquid soil moisture, resulting in  
491 increased runoff in the freezing season. During the past 40 years, parts of the permafrost  
492 changed into seasonally frozen ground and the frozen depth of the seasonally frozen  
493 ground decreased, leading to increases in the liquid soil moisture in the deep layers  
494 during the freezing season. The increase in liquid soil moisture also increased the  
495 hydraulic conductivity, which enhanced the subsurface flow. Figure 13(c) shows the  
496 seasonal pattern of runoff from the entire basin. From April to October (the thawing  
497 season), runoff in the permafrost area was much larger than in the seasonally frozen  
498 ground; however, in the freezing season runoff in the permafrost area was lower than  
499 in the seasonally frozen ground. Figure S7 in the supplementary material shows runoff

Comment [PDM74]: Delete

Comment [PDM75]: "increase in"

Comment [PDM76]: Delete

Comment [PDM77]: "area of"

Comment [PDM78]: "the inverse was true"

500 changes from a typical area (with elevations of 3500-3700 m) that featured permafrost  
501 during the period of 1971 to 1980 and that changed to seasonally frozen ground during  
502 the period of 2001 to 2010. This illustrates that the thawing of the permafrost increased  
503 the runoff in the freezing season and slowed recession processes in autumn. Figure S4

Comment [PDM79]: "1980, but degraded"

Comment [PDM80]: Delete

Comment [PDM81]: Delete

Comment [PDM82]: Delete

Comment [PDM83]: "hydrological"

504 illustrates the increase in freezing season runoff and the shift in the seasonal flow  
505 patterns simulated by the model without the frozen soil scheme.

506 Figure 13 shows the large difference in runoff variation with elevation between the  
507 freezing and thawing seasons. In the freezing season, the runoff change from the 1970s  
508 to the 2000s in the areas of seasonally frozen ground (mainly located below 3500 m,  
509 see Figure 9) was relatively small. The areas with elevations of 3500-3900 m showed  
510 larger changes in runoff. This pattern is due to the shift from permafrost to seasonally  
511 frozen ground in some areas in the elevation range of 3500 to 3900 m, as simulated by  
512 the model, particularly for sunny hillslopes (see Figure 9). This finding illustrates that  
513 a change from permafrost to seasonally frozen ground has a larger impact on the runoff  
514 than a change in frozen depth in areas of seasonally frozen ground. In the thawing  
515 season, runoff increased with elevation due to the increase in precipitation with  
516 increasing elevation, and the magnitude of the runoff increase was mainly determined  
517 by magnitude of the precipitation increase (Gao et al., 2016). Precipitation in the region  
518 with elevations below 3100 m was low, and the air temperature was high. Hence, runoff  
519 in this region was lower during 2001-2010 than during 1971-1980 because of greater  
520 evapotranspiration.

## 521 **5.2 Comparison with the previous similar studies**

522 In this study, the model simulation showed that the thawing of frozen soils led to  
523 increased freezing season runoff and base flow in the upper Heihe basin. This result is  
524 consistent with previous findings based on observations in high latitude regions  
525 (Walvoord and Striegl, 2007; Jacques and Sauchyn, 2009; Ye et al., 2009) and in

Comment [PDM84]: "large"

526 northeast China (Liu et al., 2003). However, those studies did not consider spatial  
527 variability. This study found that the impact of the frozen soil thawing on runoff varied  
528 regionally. In the upper Heihe basin (see Figure 13), the change in the freezing season  
529 runoff was strongly affected by the change from permafrost to seasonally frozen ground  
530 in the higher-elevation region and by the evaporation increase in the lower-elevation  
531 region due to rising air temperature. However, runoff at the basin scale mainly came  
532 from the higher-elevation regions.

533 This study also showed that the thawing of frozen soils increased the liquid soil  
534 moisture in the upper Heihe basin, which is consistent with the finding of Subin et al.  
535 (2013) using the CLM model to simulate northern high-latitude permafrost regions, and  
536 the findings of Cuo et al. (2015) using the VIC model to simulate 13 sites on the QTP.  
537 In contrast, Lawrence et al. (2015) found that permafrost thawing reduced soil moisture  
538 based on CLM model simulations of the global permafrost region. This finding might  
539 be related to the uncertainties in the soil water parameters and the high spatial  
540 heterogeneity of soil properties, which are difficult to consider in a global-scale model.  
541 Subin et al. (2013) and Lawrence et al. (2015) simulated the soil moisture changes in  
542 the active layer of permafrost over large areas with coarse spatial resolution. Unlike  
543 those studies, this study investigated the spatio-temporal variability in soil moisture  
544 using a high spatial resolution and analyzed the impacts of frozen soil changes.

545 Jin et al. (2009) found decreased soil moisture and runoff due to permafrost  
546 degradation based on observations at the plot scale in the source area of the Yellow  
547 River basin. These results are different from those in the present study, possibly due to

548 the difference in the hydrogeological structure and soil hydraulic parameters between  
549 the source area of the Yellow River and the upper Heihe basin. Wang et al. (2015a)  
550 estimated the increasing trend of the maximum frozen depth in the seasonally frozen  
551 ground to be  $0.04 \text{ m-decade}^{-1}$  during 1972-2006 in the Heihe River basin based on plot  
552 observations, which is consistent with the results in this study. The increase in  
553 groundwater storage illustrated in this study is also consistent with the findings of Cao  
554 et al. (2012) based on GRACE data, which showed that groundwater storage increased  
555 during the period of 2003~2008 in the upper Heihe basin.

### 556 **5.3 Uncertainty in simulation of the frozen soils**

557 Estimation of the change in permafrost area is a great challenge due to such complex  
558 factors as climatology, vegetation, and geology. Guo et al. (2013) reported that the  
559 permafrost area for the whole QTP decreased from approximately  $175.0 \times 10^4 \text{ km}^2$  in  
560 1981 to  $151.5 \times 10^4 \text{ km}^2$  in 2010, with a relative change of 13.4%. Wu et al. (2005)  
561 reported that the permafrost area decreased by 12% from 1975 to 2002 in the Xidatan  
562 basin of the QTP based on a ground penetration radar survey. Jin et al. (2006) found an  
563 area reduction of 35.6% in island permafrost in Liangdaohe, which is located along the  
564 southern portion of the Qinghai-Tibet Highway, from 1975 to 1996. Compared with the  
565 borehole observations by Wang et al. (2013) shown in Figure 2, our model slightly  
566 overestimated the soil temperature in permafrost areas, possibly leading to an  
567 overestimation of the rate of permafrost area reduction.

568 There were two major uncertainties in the frozen soils simulation: uncertainty in the  
569 simulation of the land surface energy balance and uncertainty in the simulation of the

570 soil heat-water transfer processes (Wu et al., 2016). Uncertainty in the land surface  
571 energy balance simulation might result from uncertainty in the radiation and surface  
572 albedo estimates due to the complex topography, vegetation cover and soil moisture  
573 distribution, thereby introducing uncertainties into the estimated ground temperature  
574 and soil heat flux. The uncertainty in the simulation of soil heat-water transfer processes  
575 might result from the soil water and heat parameters and the bottom boundary  
576 conditions of heat flux. For example, the soil depth and the fraction of rock in soil can  
577 greatly affect the ground temperature simulation. Permafrost degradation is closely  
578 related to the thermal properties of rocks and soils, the geothermal flow and the initial  
579 ground temperature and soil ice conditions. Sub-grid topography may also affect the  
580 frozen soil simulation. For example, active layer thickness is different between the low-  
581 elevation valleys and higher-elevation slopes due to the temperature inversion caused  
582 by the accumulation of cold air in valleys (Bonnaventure et al., 2012; Zhang et al., 2013;  
583 O'Neill et al., 2015). The laterally advected heat flux may increase the thawing of  
584 permafrost, especially in areas with high groundwater flow rates (Kurylyk et al., 2016;  
585 Sjöberg et al., 2016). Not considering the lateral heat flux may lead to an  
586 underestimation of talik development and thawing rates of permafrost. In addition,  
587 uncertainties in the input data, particularly solar radiation (which is estimated using  
588 interpolated sunshine hour data from a limited number of observational stations) and  
589 precipitation (which is also interpolated based on observations at these stations), may  
590 also influence the results of the model simulation. Due to the complexity of the  
591 distributed model and the large number of model parameters, quantifying the overall

**Comment [PDM85]:** " In areas with high groundwater flow rates , laterally advected heat flux may increase the thawing of permafrost"

592 simulation uncertainty is challenging. This work will be done in a future study.

Comment [PDM86]: "challenging, b  
is part of our ongoing research."

## 593 6. Conclusions

594 This work carefully validated a distributed hydrological model coupled with  
595 cryospheric processes in the upper Heihe River basin using available observations of  
596 soil moisture, soil temperature, frozen depth, actual evaporation and streamflow  
597 discharge. Based on the model simulations from 1971 to 2013 in the upper Heihe River,  
598 the long-term changes in frozen soils were investigated, and the effects of the frozen  
599 soil changes on the hydrological processes were explored. Based on these analyses, we  
600 have reached the following conclusions:

601 (1) The model simulation suggests that 8.8% of the permafrost areas degraded into  
602 seasonally frozen grounds in the upper Heihe River basin during 1971-2013,  
603 predominantly between elevations of 3500 m and 3900 m. The results indicate that the  
604 decreasing trend of the annual maximum frozen depth of the seasonally frozen ground  
605 is  $0.032 \text{ m-decade}^{-1}$ , which is consistent with previous observation-based studies at the  
606 plot scale. Additionally, our work indicates that the increasing trend of active layer  
607 thickness in the permafrost regions is  $0.043 \text{ m-decade}^{-1}$ .

Comment [PDM87]: "ground"

Comment [PDM88]: A trend of  
increasing"

Comment [PDM89]: "of"

608 (2) The model-simulated runoff trends agree with the observed trends. In the freezing  
609 season (November-March), based on the model simulation, runoff was mainly sourced  
610 from subsurface flow, which increased significantly in the higher elevation regions  
611 where significant frozen soil changes occurred. This finding implies that the runoff  
612 increase in the freezing season is primarily caused by frozen soil changes (permafrost  
613 degradation and reduced seasonally frozen depth). In the thawing season (April-

614 October), the model simulation indicates that runoff was mainly sourced from rainfall  
615 and showed an increasing trend at higher elevations, which can be explained by the  
616 increase in precipitation. In both the freezing and thawing seasons, the model-simulated  
617 runoff decreased in the lower-elevation regions, which can be explained by increased  
618 evaporation due to rising air temperatures.

619 (3) The model-simulated changes in soil moisture and ground temperature indicate  
620 that the annual storage of liquid water increased, especially in the most recent three  
621 decades, due to frozen soil changes. The annual ice water storage in the top 0-3 m of  
622 soil showed a significant decreasing trend due to soil warming. The model simulated  
623 annual groundwater storage had an increasing trend, which is consistent with the  
624 changes observed by the GRACE satellite. Therefore, groundwater recharge in the  
625 upper Heihe basin has increased in recent decades.

626 (4) The model simulation indicated that regions where permafrost changed into  
627 seasonally frozen ground had larger changes in runoff and soil moisture than the areas  
628 covered by seasonally frozen ground throughout the study period.

629 For a better understanding of the changes in frozen soils and their impact on  
630 ecohydrology, the interactions among soil freezing-thawing processes, vegetation  
631 dynamics and hydrological processes need to be investigated in future studies. There  
632 are uncertainties in simulations of frozen soils and hydrological processes that also  
633 warrant further investigation in the future.

634

635 **Acknowledgements:** This research was supported by the major plan of “Integrated

Comment [PDM90]: Delete

Comment [PDM91]: At your discretion, I recommend acknowledging that suggestions from reviewers have substantially improved the paper.

636 Research on the Ecohydrological Processes of the Heihe Basin” (Project Nos.  
637 91225302 and 91425303) funded by the National Natural Science Foundation of China  
638 (NSFC). All data for this paper are properly cited and referred in the reference list.  
639 The model code with a working example is freely available from our website  
640 (<https://github.com/gb03/GBEHM>) or upon request from the corresponding author  
641 ([yangdw@tsinghua.edu.cn](mailto:yangdw@tsinghua.edu.cn)).

Comment [PDM92]: “cited in this paper are available from the references”

642

### 643 **References**

- 644 Bartelt P. and M. Lehning: A physical snowpack model for the swiss avalanche warning: Part I :  
645 numerical model, *Cold Regions Sci. and Tech.*, 35(3), 123-145, doi: 10.1016/S0165-  
646 232X(02)00074-5, 2002.
- 647 Bonnaventure PP, Lewkowicz AG, Kremer M, Sawada MC: A Permafrost Probability Model for the  
648 Southern Yukon and Northern British Columbia, Canada, *Permafrost and Periglac. Process.*, 23,52-  
649 68, doi: 10.1002/ppp.1733, 2012.
- 650 Cao Y., Nan Z. and Hu X.: Estimating groundwater storage changes in the Heihe river basin using  
651 GRACE, in: *IEEE International Geoscience and Remote Sensing Symposium (IGARSS)*, Munich,  
652 Germany, 22–27 July 2012, 798-801, 2012.
- 653 Chen, R., Lu, S., Kang, E., Ji, X., Zhang, Z., Yang, Y., Qing, W.: A distributed water-heat coupled model  
654 for mountainous watershed of an inland river basin of Northwest China (I) model structure and  
655 equations, *Environ. Geol.*, 53, 1299-1309, doi: 10.1007/s00254-007-0738-2, 2008.
- 656 Cheng, G. and Jin, H.: Permafrost and groundwater on the Qinghai-Tibet Plateau and in northeast China,  
657 *Hydrogeol. J.*, 21, 5-23, doi: 10.1007/s10040-012-0927-2, 2013.

658 Cheng, G., Li, X., Zhao, W., Xu, Z., Feng, Q., Xiao, S., Xiao, H.: Integrated study of the water-  
659 ecosystem-economy in the Heihe River Basin. *Nat. Sci. Rev.*, 1(3), 413-428, doi:  
660 10.1093/nsr/nwu017, 2014.

661 Cheng, G., and Wu T.: Responses of permafrost to climate change and their environmental significance,  
662 Qinghai-Tibet Plateau, *J. Geophys. Res.*, 112, F02S03, doi:10.1029/2006JF000631, 2007.

663 Cherkauer, K. A., and D. P. Lettenmaier: Hydrologic effects of frozen soils in the upper Mississippi River  
664 basin, *J. Geophys. Res.*, 104, 19,599-19,610, doi: 10.1029/1999JD900337, 1999.

665 Cong Z T, Yang D W, Gao B, et al.: Hydrological trend analysis in the Yellow River basin using a  
666 distributed hydrological model, *Water Resour Res*, 45: W00A13, doi: 10.1029/2008WR006852,  
667 2009

668 Cuo, L., Y. Zhang, F. Zhu, and L. Liang.: Characteristics and changes of streamflow on the Tibetan  
669 Plateau: A review, *J. Hydrol.: Reg. Stud.*, 2, 49-68, doi: 10.1016/j.ejrh.2014.08.004, 2014.

670 Cuo, L., Y. Zhang, T. J. Bohn, L. Zhao, J. Li, Q. Liu, and B. Zhou: Frozen soil degradation and its effects  
671 on surface hydrology in the northern Tibetan Plateau, *J. Geophys. Res. Atmos.*, 120,  
672 doi:10.1002/2015JD023193, 2015.

673 Duan L., Man X., Kurylyk B. L. and Cai T.: Increasing winter baseflow in response to permafrost thaw  
674 and precipitation regime shifts in northeastern China, *Water*, 9(1), 25, doi:10.3390/w9010025, 2017.

675 Endrizzi S, Gruber S, Dall'Amico M, and R. Rigon: GEOTop 2.0: simulating the combined energy and  
676 water balance at and below the land surface accounting for soil freezing, snow cover and terrain  
677 effects, *Geosci. Model Dev.*, 7: 2831-2857, doi:10.5194/gmd-7-2831-2014, 2014.

678 Fan, W.: Heihe 1km LAI production, Heihe Plan Science Data Center at Lanzhou,  
679 doi:10.3972/heihe.090.2014.db, 2014.

680 Farouki, O.T.: The thermal properties of soils in cold regions, *Cold Regions Sci. and Tech.*, 5, 67-75, doi:  
681 10.1016/0165-232X(81)90041-0, 1981.

682 Flerchinger G., Saxton K.: Simultaneous heat and water model of a freezing snow-residue-soil system I.  
683 Theory and development, *Trans. ASAE*, 32, 565-571, doi: 10.13031/2013.31040, 1989.

684 Gao B., Qin Y., Wang YH, Yang DW, and Zheng YR: Modeling Ecohydrological Processes and Spatial  
685 Patterns in the Upper Heihe Basin in China, *Forests*, 7(1),10, doi:10.3390/f7010010, 2016.

686 Guo, D., and H. Wang: Simulation of permafrost and seasonally frozen ground conditions on the Tibetan  
687 Plateau, 1981–2010, *J. Geophys. Res. Atmos.*, 118, 5216-5230, doi:10.1002/jgrd.50457, 2013.

688 Hinzman, L.D., C.J. Deal, A.D. McGuire, S.H. Mernild, I.V. Polyakov, and J.E. Walsh: Trajectory of  
689 the Arctic as an integrated system, *Ecol. Appl.*, 23(8),1837-1868, doi:10.1890/11-1498.1, 2013.

690 Jacques St., J.-M., and Sauchyn D. J.: Increasing winter baseflow and mean annual streamflow from  
691 possible permafrost thawing in the Northwest Territories, Canada, *Geophys. Res. Lett.*, 36, L01401,  
692 doi:10.1029/2008GL035822, 2009.

693 Jarvis, A., Reuter, H.I., Nelson, A., Guevara, E.: Hole-filled seamless SRTM data, Version 4,  
694 International Centre for Tropical Agriculture (CIAT), 2008.

695 Jin, H., He, R., Cheng, G., Wu, Q., Wang, S., Lu, L. and Chang X.: Changes in frozen ground in the  
696 Source Area of the Yellow River on the Qinghai–Tibet Plateau, China, and their eco-environmental  
697 impacts, *Environ. Res. Lett.*, 4(4), 045206, doi:10.1088/1748-9326/4/4/045206, 2009.

698 Jin, H.J., Zhao, L., Wang, S.L., Jin, R.: Thermal regimes and degradation modes of permafrost along  
699 the Qinghai–Tibet Highway, *Science in China D: Earth Sciences*, 49 (11), 1170-1183, 2006.

700 Jordan R.: A one-dimensional temperature model for a snow cover, Technical Documentation for  
701 SNTHERM.89, Cold Regions Research and Engineering Lab, Hanover NH, 49 pp., 1991.

702 Kurylyk, B. L., M. Hayashi, W. L. Quinton, J. M. McKenzie, and C. I. Voss: Influence of vertical and  
703 lateral heat transfer on permafrost thaw, peatland landscape transition, and groundwater flow, *Water*  
704 *Resour. Res.*, 52, 1286-1305, doi:10.1002/2015WR018057, 2016.

705 Lawrence, D.M., C.D. Koven, S.C. Swenson, W.J. Riley, and A.G. Slater: Permafrost thaw and resulting  
706 soil moisture changes regulate projected high-latitude CO<sub>2</sub> and CH<sub>4</sub> emissions, *Environ. Res. Lett.*,  
707 10, doi:10.1088/1748-9326/10/9/094011, 2015.

708 Li, D.L., Zhong, H.L., Wu, Q.B., Zhang, Y.J., Hou, Y.L., Tang, M.C.: Analyses on changes of surface  
709 temperature over Qinghai–Xizang Plateau, *Plateau Meteorology*, 24, 291-298, 2005 (in Chinese).

710 Li, X., Cheng, G.D., Liu, S.M., Xiao, Q., Ma, M.G., Jin, R., Che, T., Liu, Q.H., Wang, W.Z., Qi, Y., Wen,  
711 J.G., Li, H.Y., Zhu, G.F., Guo, J.W., Ran, Y.H., Wang, S.G., Zhu, Z.L., Zhou, J., Hu, X.L., Xu, Z.W.:  
712 Heihe Watershed Allied Telemetry Experimental Research (HiWATER): Scientific Objectives and  
713 Experimental Design, *B. Am. Meteorol. Soc.*, 94(8), 1145-1160, doi: 10.1175/BAMS-D-12-00154.1,  
714 2013.

715 Liu, X. and Chen, B.: Climate warming in the Tibetan Plateau during recent decades, *Int. J. Climatol.*,  
716 20(1), 1729-1742, doi: 10.1002/1097-0088(20001130)20:14<1729::AID-JOC556>3.0.CO;2-, 2000.

717 Liu, S., Xu Z., Wang W., Bai J., Jia Z., Zhu M., and Wang J.: A comparison of eddy-covariance and large  
718 aperture scintillometer measurements with respect to the energy balance closure problem, *Hydrol.*  
719 *Earth Syst. Sc.*, 15(4), 1291-1306, doi:10.5194/hess-15-1291-2011, 2011.

720 Liu J., N. Hayakawab, Lu M., Dong S., and Yuan J.: Hydrological and geocryological response of winter  
721 streamflow to climate warming in Northeast China, *Cold Regions Sci.and Tech.*, 37,15-24, doi:  
722 10.1016/S0165-232X(03)00012-0, 2003.

723 Wu T., Li S., Cheng G. and N Z.: Using ground-penetrating radar to detect permafrost degradation in  
724 the northern limit of permafrost on the Tibetan Plateau, *Cold Regions Sci.and Tech.*, 41, 211-219,

725 2005, doi:10.1016/j.coldregions.2004.10.006.

726 Niu L., Ye B., Li J., and Sheng Y.: Effect of permafrost degradation on hydrological processes in typical  
727 basins with various permafrost coverage in Western China, *China Earth Sci.*, 54(4), 615-624, doi:  
728 10.1007/s11430-010-4073-1, 2011.

729 Oerlemans, J. and Knap, W.H.: A 1 year record of global radiation and albedo in the ablation zone of  
730 Morteratschgletscher, Switzerland, *J. Glaciol.*, 44, 231-238, doi: 10.3198/1998JoG44-147-231-238,  
731 1998.

732 Oerlemans, J.: *Glaciers and Climate Change*, Lisse: Swets & Zeitlinger, 2001.

733 Oleson, K.W., Lawrence, D.M., Bonan, G.B., Flanner, M.G., Kluzek, E., Lawrence, P.J., Levis, S.,  
734 Swenson, S.C., Thornton, P.E., Dai, A., Decker, M., Dickinson, R., Feddema, J., Heald, C.L.,  
735 Hoffman, F., Lamarque, J., Mahowald, N., Niu, G., Qian, T., Randerson, J., Running, S., Sakaguchi,  
736 K., Slater, A., Stöckli, R., Wang, A., Yang, Z., Zeng, X., Zeng, X.: Technical Description of version  
737 4.0 of the Community Land Model (CLM), NCAR Technical Note NCAR/TN-47+STR, National  
738 Center for Atmospheric Research, Boulder, CO, 257 pp., 2010.

739 Qiu J.: Thawing permafrost reduces river runoff, *Nature*, doi:10.1038/nature.2012.9749, 2012.

740 Ou, C., B. Leblon, Y. Zhang, A. LaRocque, K. Webster, and J. McLaughlin: Modelling and mapping  
741 permafrost at high spatial resolution using Landsat and RADARSAT images in northern Ontario,  
742 Canada: Part 1 - Model calibration, *International Journal of Remote Sensing*, doi:  
743 10.1080/01431161.2016.1157642, 2016.

744 O'Neill, H. B., Burn, C. R., Kokelj, S. V. & Lantz, T. C.: 'Warm' tundra: atmospheric and near-surface  
745 ground temperature inversions across an alpine treeline in continuous permafrost, western arctic,  
746 Canada. *Permafrost and Periglac. Process.* 26, 103–118, doi: 10.1002/ppp.1838., 2015.

747 Rawlins M., Lammers R., Frohling S., Fekete B. and Vorosmarty C.: Simulating pan-Arctic runoff with  
748 a macro-scale terrestrial water balance model, *Hydrol. Process.*, 17, 2521-2539, doi:

749 10.1002/hyp.1271, 2003.

750 Rawlins, M.A., D.J. Nicolsky, K.C. McDonald, and V.E. Romanovsky: Simulating soil freeze/thaw  
751 dynamics with an improved pan-Arctic water balance model, *J. Adv. Model. Earth Syst.*, 5:659-675,  
752 doi:10.1002/jame.20045, 2013.

753 Rigon R., Bertoldi G., and Over TM: GEOTop: A distributed hydrological model with coupled water  
754 and energy budgets, *J. Hydrometeorol.*, 7, 371–388, doi: 10.1175/JHM497.1, 2006.

755 Schuur, E.A.G., A.D. McGuire, C. Schädel, G. Grosse, J.W. Harden, D.J. Hayes, G. Hugelinius, C.D.  
756 Koven, P. Kuhry, D.M. Lawrence, S.M. Natali, D. Olefeldt, V.E. Romanovsky, K. Schaefer, M.R.  
757 Turetsky, C.C. Treat, and J.E. Vonk: Climate change and the permafrost carbon feedback, *Nature*  
758 520,171-179 doi:10.1038/nature14338, 2015.

759 Sellers, P.J.: Canopy reflectance, photosynthesis, and transpiration, *Int. J. Remote Sens.*, 8, 1335-1372,  
760 doi: 10.1080/01431168508948283, 1985.

761 Sellers, P.J.; Randall, D.A.; Collatz, G.J.; Berry, J.A.; Field, C.B.; Dazlich, D.A.; Zhang, C.; Collelo,  
762 G.D.; Bounoua, L.: A Revised Land Surface Parameterization (SiB2) for Atmospheric GCMS.  
763 Part I: Model Formulation, *J. Clim.*, 9, 676-705, doi: 10.1175/1520-  
764 0442(1996)009<0676:ARLSPF>2.0.CO;2, 1996.

765 Sjöberg, Y., E. Coon, A. B. K. Sannel, R. Pannetier, D. Harp, A. Frampton, S. L. Painter, and S. W. Lyon:  
766 Thermal effects of groundwater flow through subarctic fens: A case study based on field  
767 observations and numerical modeling, *Water Resour. Res.*, 52, 1591-1606,  
768 doi:10.1002/2015WR017571, 2016.

769 Song X., Brus DJ, Liu F., Li D., Zhao Y., Yang J. and Zhang G.: Mapping soil organic carbon content by  
770 geographically weighted regression: A case study in the Heihe River Basin, China, *Geoderma*,

771 261,11–22, doi: 10.1016/j.geoderma.2015.06.024, 2016.

772 Strahler A N: Quantitative analysis of watershed geomorphology, *Eos, Transactions American*  
773 *Geophysical Union*, 38(6), 913-920, doi: 10.1029/TR038i006p00913, 1957.

774 Subin Z.M., Koven C.D., Riley W.J., Torn M.S., Lawrence D.M. and Swenson S.C.: Effects of Soil  
775 Moisture on the Responses of Soil Temperatures to Climate Change in Cold Regions, *J. Clim.*,  
776 26,3139-3158, doi: 10.1175/JCLI-D-12-00305.1, 2013.

777 Toon, O.B., McKay, C.P., Ackerman, T.P., and Santhanam, K.: Rapid calculation of radiative heating  
778 rates and photodissociation rates in inhomogeneous multiple scattering atmospheres, *J. Geophys.*  
779 *Res.* 94(D13), 16,287-16,301, doi: 10.1029/JD094iD13p16287, 1989.

780 Walter W. Immerzeel, Ludovicus P. H. van Beek, and Marc F. P. Bierkens.: Climate Change Will Affect  
781 the Asian Water Towers, *Science*, 328, 1382-1385, doi: 10.1126/science.1183188, 2010.

782 Walvoord, M. A. and B. L. Kurylyk: Hydrologic Impacts of Thawing Permafrost—A Review, *Vadose*  
783 *Zone J.*, doi:10.2136/vzj2016.01.0010, 2016.

784 Walvoord, M. A., and R. G. Striegl: Increased groundwater to stream discharge from permafrost thawing  
785 in the Yukon River basin: Potential impacts on lateral export of carbon and nitrogen, *Geophys. Res.*  
786 *Let.*, 34, L12402, doi:10.1029/2007GL030216, 2007.

787 Wang, L., Koike, T., Yang, K., Jin, R., Li, H.: Frozen soil parameterization in a distributed biosphere  
788 hydrological model, *Hydrol. Earth Syst. Sc.*, 14(3), 557-571, doi: 10.5194/hess-14-557-2010, 2010.

789 Wang Q., Zhang T., Wu J., et al.: Investigation of permafrost distribution over the upper reaches of the  
790 Heihe River in the Qilian Mountains, *Journal of Glaciology and Geocryology*, 35(1), 19-29, 2013  
791 (in Chinese).

792 Wang Q., Zhang T., Peng X., Cao B., and Wu Q.: Changes of soil thermal regimes in the Heihe River

793 Basin over Western China, *Arct., Antarct., and Alpine Res.*, 47(2), 231-241, doi:  
794 10.1657/AAAR00C-14-012, 2015a.

795 Wang, Y., Yang, D., Lei, H. and Yang, H.: Impact of cryosphere hydrological processes on the river runoff  
796 in the upper reaches of Heihe River, *J. Hydraul. Eng.*, 46, 1064-1071, 2015b (In Chinese).

797 Wang, Y., Yang, H., Yang, D., Qin Y., Gao B. and Cong ZT.: Spatial interpolation of daily precipitation  
798 in a high mountainous watershed based on gauge observations and a regional climate model  
799 simulation, *J. Hydrometeorol.*, 18, 845-862, 2017, doi: 10.1175/JHM-D-16-0089.1.

800 Woo, M.-K., Kane, D. L., Carey, S. K. and Yang, D.: Progress in permafrost hydrology in the new  
801 millennium, *Permafrost Periglac. Process.*, 19, 237-254, doi:10.1002/ppp.613, 2008.

802 Woo M K.: *Permafrost Hydrology*, Springer-Verlag, Berlin Heidelberg, 2012.

803 Wu, B.F., Yan, N.N., Xiong, J., Bastiaanssen, W., Zhu, W.W., Stein, A.: Validation of ETWatch using  
804 field measurements at diverse landscapes: A case study in Hai Basin of China. *J. Hydrol.*, 436, 67-  
805 80, doi: 10.1016/j.jhydrol.2012.02.043, 2012.

806 Wu, B.F.: *Monthly Evapotranspiration Datasets (2000–2012) with 1 km Spatial Resolution over the*  
807 *Heihe River Basin*, Heihe Plan Science Data Center at Lanzhou, China, doi:  
808 10.3972/heihe.115.2013.db, 2013.

809 Wu, M., Jansson P. E., Tan X., Wu J., and Huang, J.: Constraining parameter uncertainty in simulations  
810 of water and heat dynamics in seasonally frozen soil using limited observed data, *Water*, 8(2), 64,  
811 doi:10.3390/w8020064, 2016.

812 Wu, Q., Zhang T. and Liu Y.: Permafrost temperatures and thickness on the Qinghai-Tibet Plateau, *Glob.*  
813 *Planet. Change*, 72, 32-38, doi: 10.1016/j.gloplacha.2010.03.001, 2010.

814 Yang, D.W., Gao, B., Jiao, Y., Lei, H.M., Zhang, Y.L., Yang, H.B., Cong, Z.T.: A distributed scheme

815 developed for eco-hydrological modeling in the upper Heihe River, China Earth Sci., 58(1), 36-45,  
816 doi: 10.1007/s11430-014-5029-7, 2015.

817 Yang, D.W., Herath, S., and Musiaka, K.: Development of a geomorphology-based hydrological model  
818 for large catchments, Annu. J. Hydraul. Eng., 42, 169-174, doi: 10.2208/prohe.42.169, 1998.

819 Yang, D.W., Herath, S., and Musiaka, K.: A hillslope-based hydrological model using catchment area  
820 and width functions, Hydrol. Sci. J., 47, 49-65, doi: 10.1080/02626660209492907, 2002.

821 Yang, M., F. E. Nelson, N. I. Shiklomanov, D. Guo, and G. Wan, Permafrost degradation and its  
822 environmental effects on the Tibetan Plateau: A review of recent research, Earth Sci. Rev., 103, 31-  
823 44, doi: 10.1016/j.earscirev.2010.07.002, 2010.

824 Ye, B., D. Yang, Z. Zhang, and D. L. Kane: Variation of hydrological regime with permafrost coverage  
825 over Lena Basin in Siberia, J. Geophys. Res., 114, D07102, doi:10.1029/2008JD010537, 2009.

826 Zhao, L., C. L. Ping, D. Q. Yang, G. D. Cheng, Y. J. Ding, and S. Y. Liu: Changes of climate and  
827 seasonally frozen ground over the past 30 years in Qinghai-Xizang (Tibetan) Plateau, China, Global  
828 Planet. Change, 43, 19-31, doi: 10.1016/j.gloplacha.2004.02.003, 2004.

829 Zhang, Y.L., Cheng, G.D., Li, X., Han, X.J., Wang, L., Li, H.Y., Chang, X.L., Flerchinger, G.N.:  
830 Coupling of a simultaneous heat and water model with a distributed hydrological model and  
831 evaluation of the combined model in a cold region watershed, Hydrol. Process., 27(25), 3762-3776,  
832 doi: 10.1002/hyp.9514, 2013.

833 Zhang, Y., Ohata, T., and Kadota, T.: Land-surface hydrological processes in the permafrost region of the  
834 eastern Tibetan Plateau, J. Hydrol., 283, 41-56, doi: 10.1016/S0022-1694(03)00240-3, 2003.

835 Zhang, Y., X. Wang, R. Fraser, I. Olthof, W. Chen, D. McLennan, S. Ponomarenko, and W. Wu: Modelling  
836 and mapping climate change impacts on permafrost at high spatial resolution for an Arctic region

837 with complex terrain, *The Cryosphere*, 7, 1121-1137, doi:10.5194/tc-7-1121-2013, 2013.

838 Zhou, J.H. and Zheng, Y.R.: Vegetation Map of the upper Heihe basin, Version 2.0, Heihe Plan Science

839 Data Center at Lanzhou, China, doi:10.3972/heihe.426.2014.db, 2014.

840

841 **Figure caption:**

842 Figure 1. The Study area, hydrological stations, borehole observation and flux tower stations.

843 Figure 2. Model structure and vertical discretization of soil column.

844 Figure 3. Comparison of the simulated and the observed soil temperature at borehole observation

845 sites, and the observed data is provided by Wang et al. (2013).

846 Figure 4. Daily soil temperature at the Qilian station: (a) observation; (b) simulation; (c) difference

847 (simulation - observation).

848 Figure 5. Comparison of the simulated and observed daily frozen depths during the period of 2002-

849 2014 at: (a) the Qilian station, (b) the Yeniugou station.

850 Figure 6. Comparison of the simulated and the observed daily river discharge at: (a) the Yingluoxia

851 Gauge, (b) the Qilian Gauge, and (c) the Zhamashike Gauge. For each gauge, the upper and lower

852 panels show the calibration and validation periods, respectively. Nash-Sutcliffe efficiency and

853 relative error coefficients are indicated.

854 Figure 7. Simulated ground temperature changes in: (a) the freezing season (from November to

855 March) (b) the thawing season (from April to October).

856 Figure 8. Change of the frozen soils in the upper Heihe basin: (a) areas of permafrost and basin

857 averaged annual air temperature; (b) the basin averaged annual maximum depths of seasonally

858 frozen ground and thaw above permafrost.

859 Figure 9. Distribution of permafrost and seasonally frozen ground for two periods: (a) 1971-1980  
860 and (b) 2001-2010; (c) Area where permafrost degraded to seasonally frozen ground from (a) to (b);  
861 Percentage of permafrost area with respect to elevation on the (d) sunny and (e) the shaded slopes  
862 for the two periods. Note that (d) and (e) share a legend.

863 Figure 10. Spatially averaged monthly ground temperatures simulated from 1971 to 2013 for two  
864 elevation intervals: (a) seasonally frozen ground between 3300 and 3500 m; (b) permafrost that  
865 degraded to seasonally frozen ground between 3500 and 3700 m.

866 Figure 11. Runoff and simulated evapotranspiration in (a) the freezing season and (b) the thawing  
867 season. Trend lines are for simulated data. The up two panels are for freezing season and the lower  
868 two panels are for thawing season.

869 Figure 12. Basin averaged annual water storage (equivalent water depth) changes simulated over  
870 the period of 1971 to 2013 for: (a) liquid water in the top layer of the ground (0-3 m); (b) ice in the  
871 top layer of the ground (0-3 m); (c) and ground water.

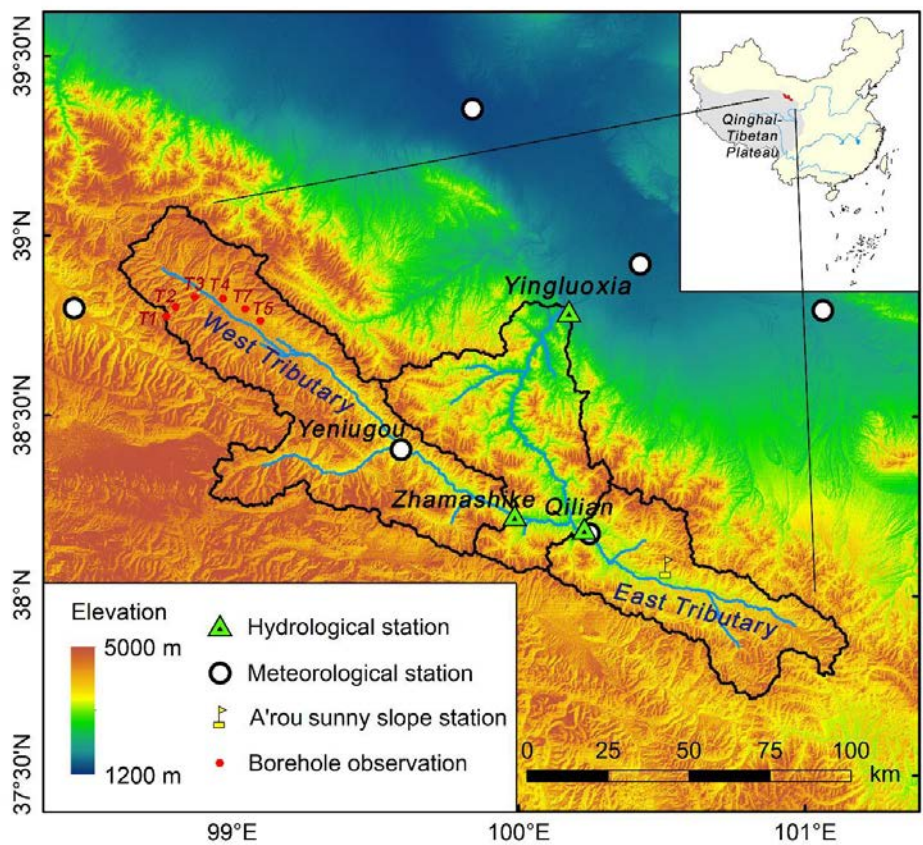
872 Figure 13. Model simulated runoff changes from the 1971-1980 period to the 2001-2010 period  
873 with elevation for (a) the freezing season and (b) the thawing season, and (c) monthly averaged  
874 seasonal runoff in permafrost and seasonally frozen ground for the period of 2001-2010.

875

876

877

878



879

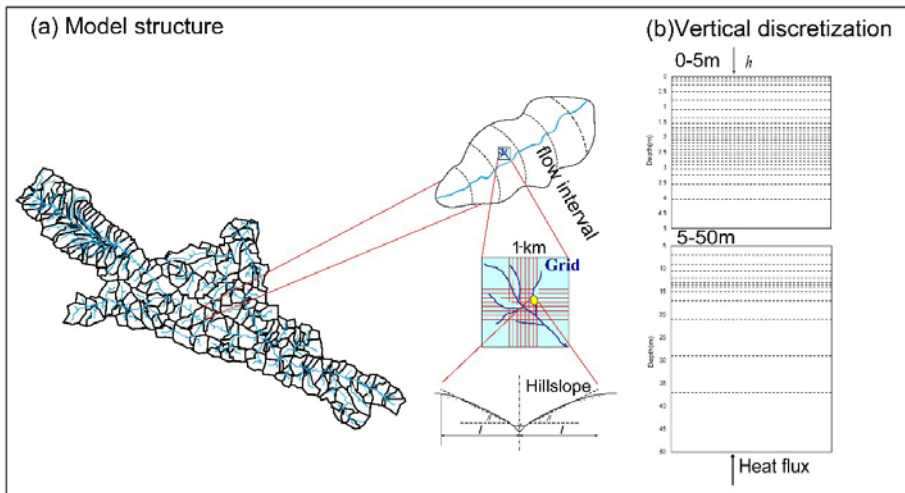
880 Figure 1. The Study area, hydrological stations, borehole observation and flux tower

881

stations.

882

Comment [PDM93]: Change color of boreholes sites to black so they are immediately visible. Figure looks great!

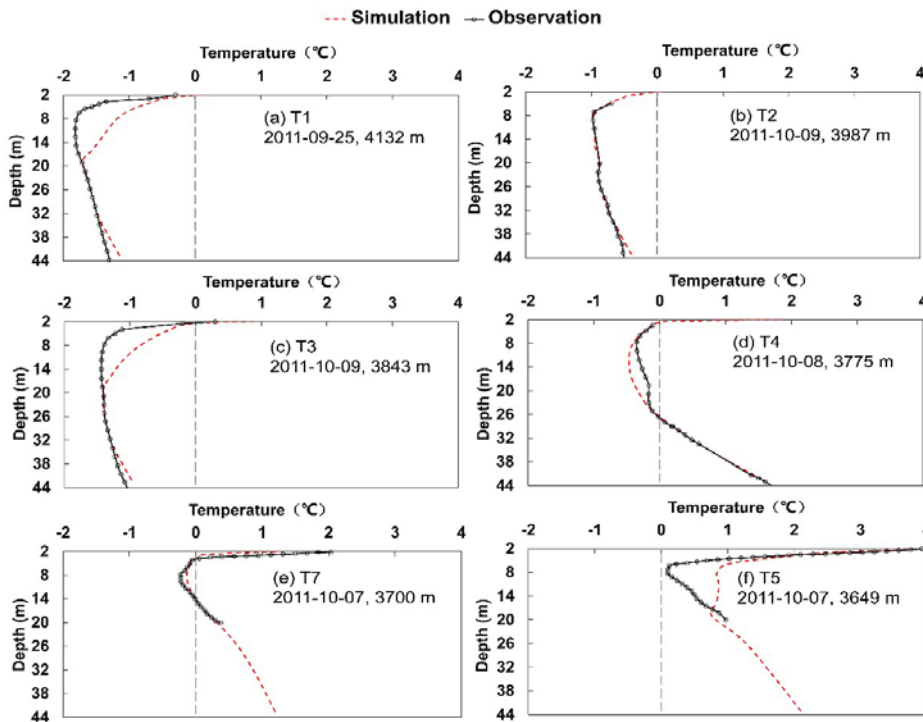


883

884 Figure 2. Model structure and vertical discretization of soil column.

885

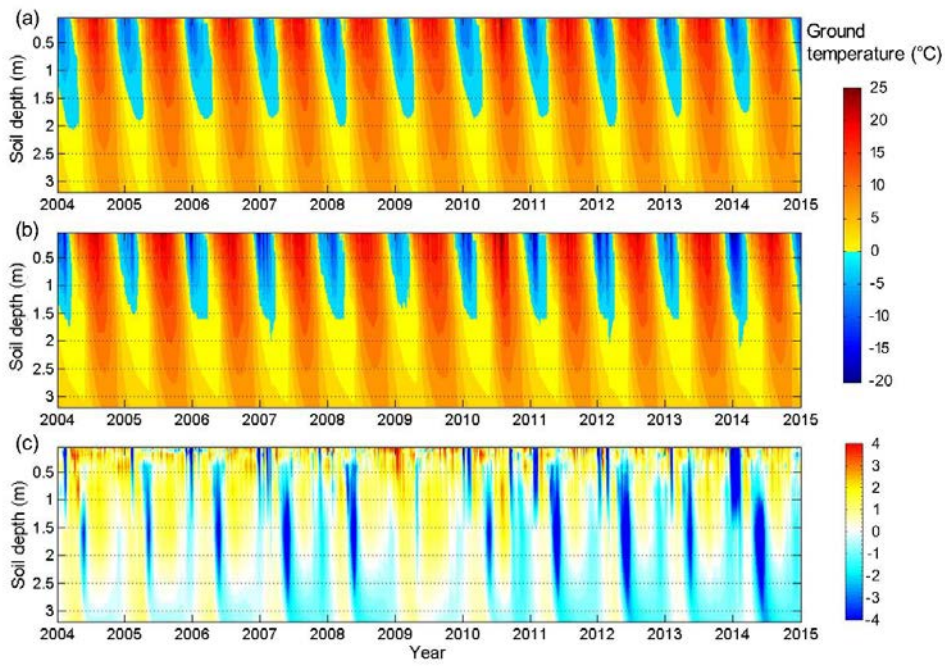
886



887

888 Figure 3. Comparison of the simulated and the observed soil temperature at borehole

889 observation sites, and the observed data is provided by Wang et al. (2013).



890

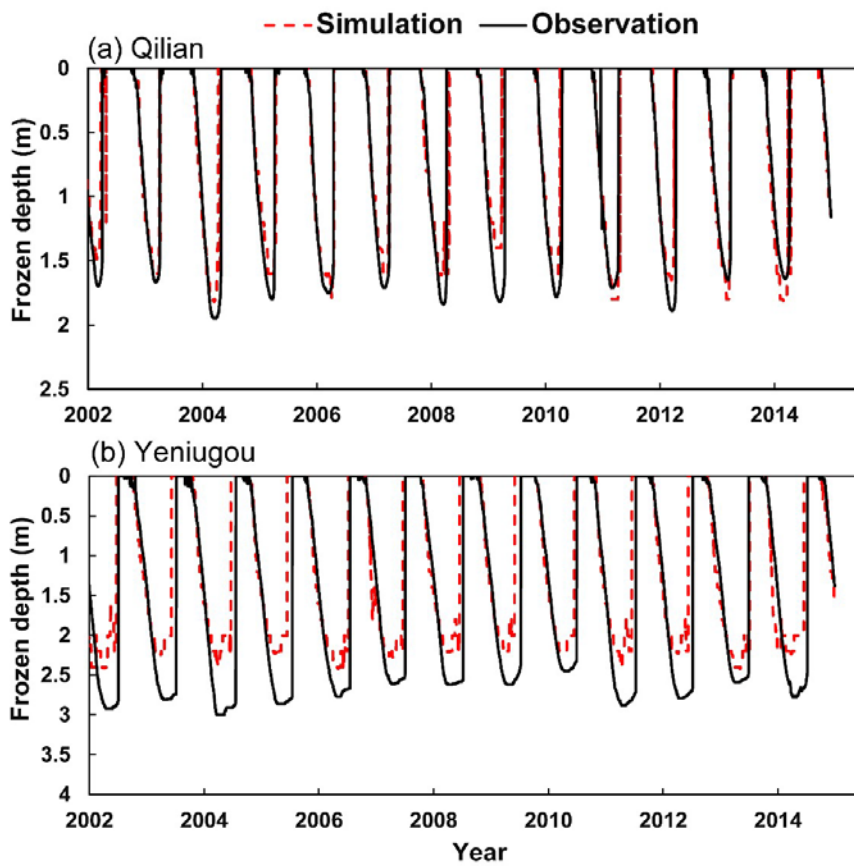
891 Figure 4. Daily soil temperature at the Qilian station: (a) observation; (b) simulation;

892

(c) difference (simulation - observation).

893

894



895

896 Figure 5. Comparison of the simulated and observed daily frozen depths during the

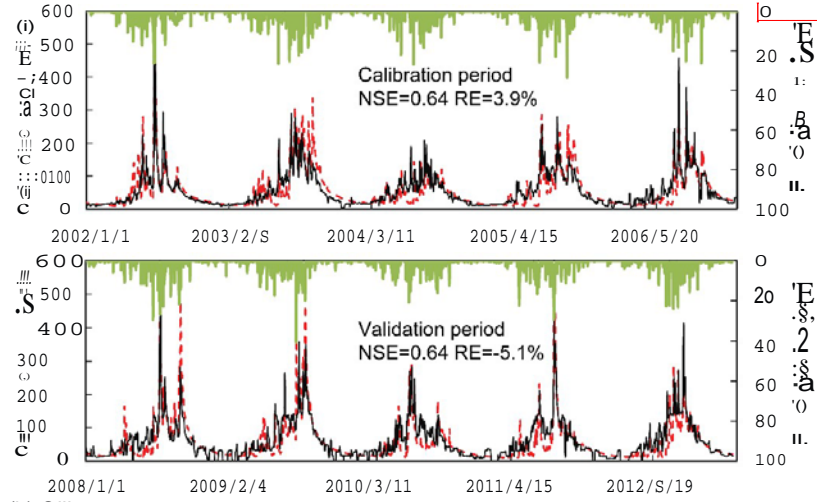
897 period of 2002-2014 at: (a) the Qilian station, (b) the Yeniugou station.

898

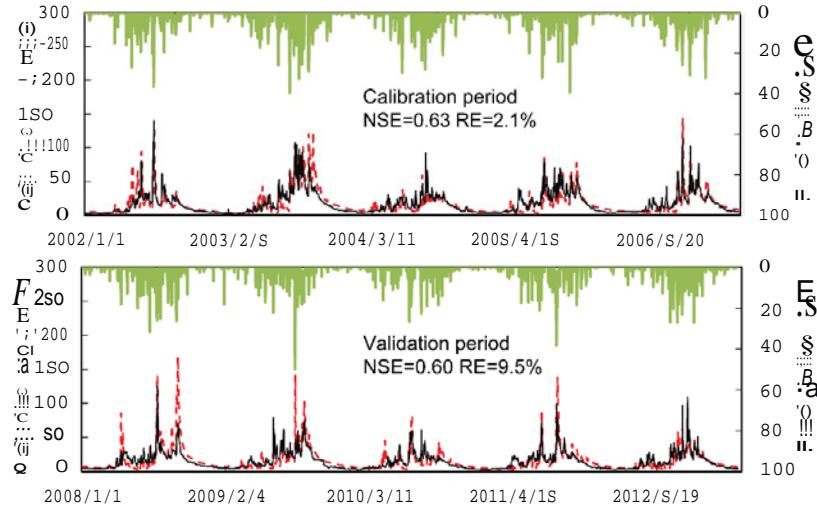
899

Simulation — Observation — Precipitation

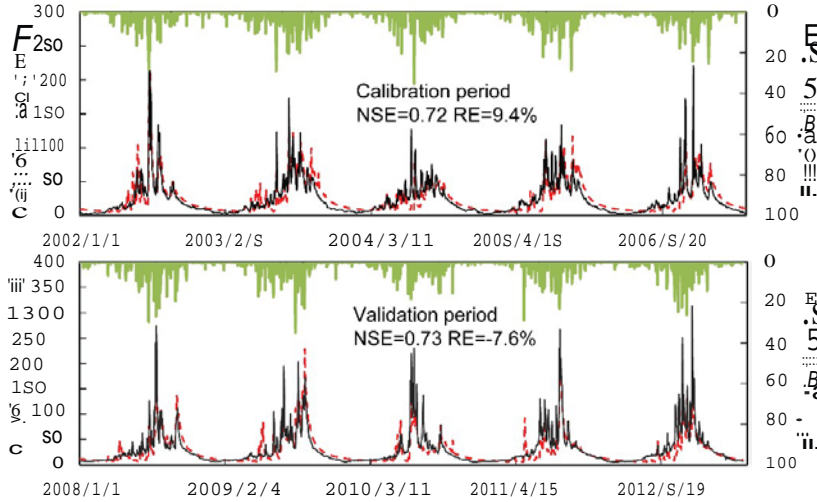
(a) Yingluoxia



(b) Qilian



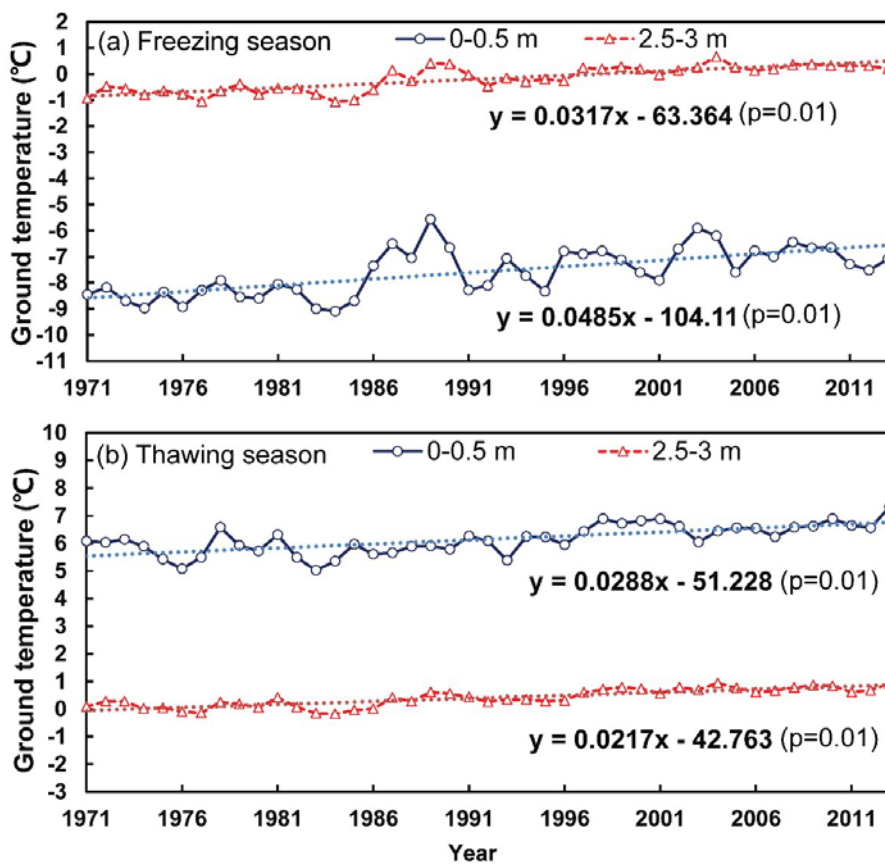
(c) Zhamashike



Comment [PDM94]: Not sure why the figure looks like this after I exported to Word, but anyway, please change "(m<sup>2</sup>/s)" to "(m<sup>3</sup>·s<sup>-1</sup>)" in axis titles.

901 Figure 6. Comparison of the simulated and the observed daily river discharge at: (a) the  
 902 Yingluoxia Gauge, (b) the Qilian Gauge, and (c) the Zhamashike Gauge. For each  
 903 gauge, the upper and lower panels show the calibration and validation periods,  
 904 respectively. Nash-Sutcliffe efficiency and relative error coefficients are indicated.

905  
 906



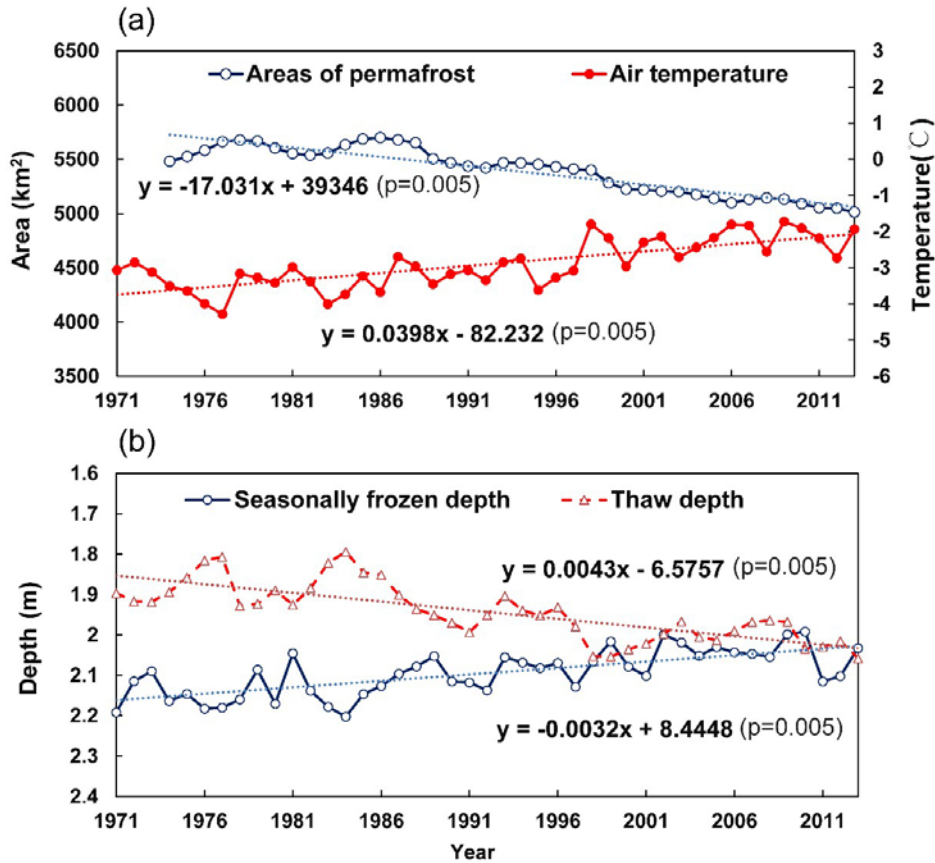
907  
 908 Figure 7. Simulated ground temperature changes in: (a) the freezing season (from  
 909 November to March) (b) the thawing season (from April to **October**).

910  
 911

Comment [PDM95]: "October). Res from linear regressions are indicated."

912

913



914

915 Figure 8. Change of the frozen soils in the upper Heihe basin: (a) areas of permafrost

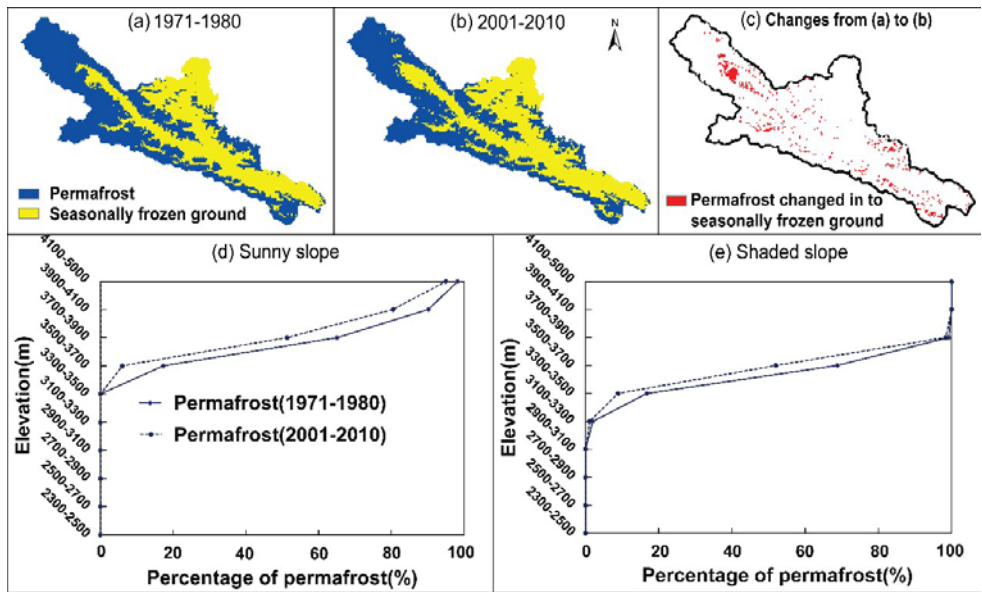
916 and basin averaged annual air temperature; (b) the basin averaged annual maximum

917 depths of seasonally frozen ground and thaw above permafrost.

918

919

Comment [PDM96]: "permafrost. Results from linear regressions are indicated."



920

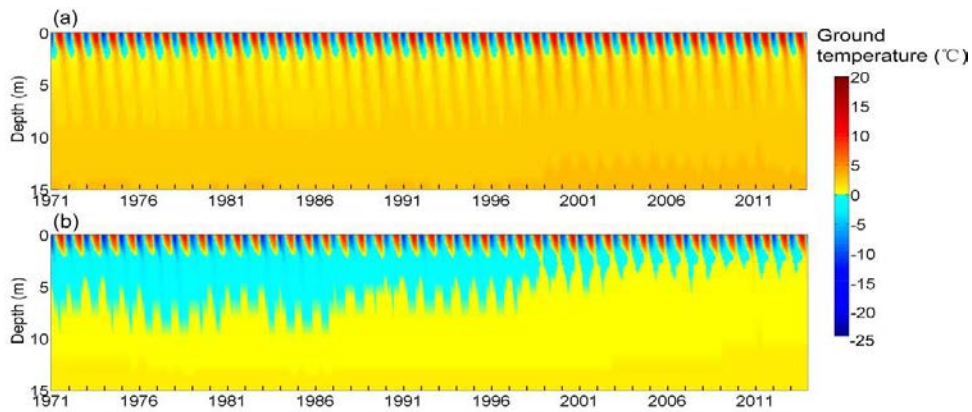
921 Figure 9. Distribution of permafrost and seasonally frozen ground for two periods: (a)

922 1971-1980 and (b) 2001-2010; (c) Area where permafrost degraded to seasonally

923 frozen ground from (a) to (b); Percentage of permafrost area with respect to elevation

924 on the (d) sunny and (e) the shaded slopes for the two periods. Note that (d) and (e)

925 share a legend.



926

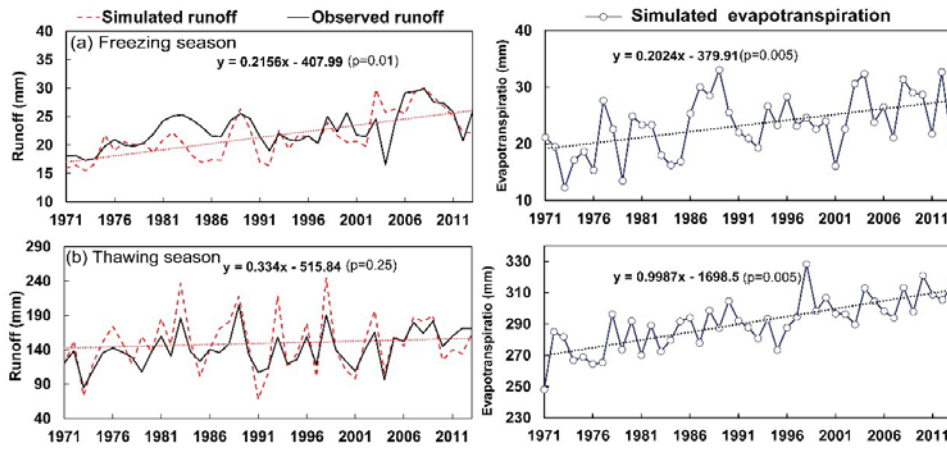
927 Figure 10. Spatially averaged monthly ground temperatures simulated from 1971 to

928 2013 for two elevation intervals: (a) seasonally frozen ground between 3300 and 3500

929 m; (b) permafrost that degraded to seasonally frozen ground between 3500 and 3700 m.

930

931



932

933 Figure 11. Runoff and simulated evapotranspiration in (a) the freezing season and (b)

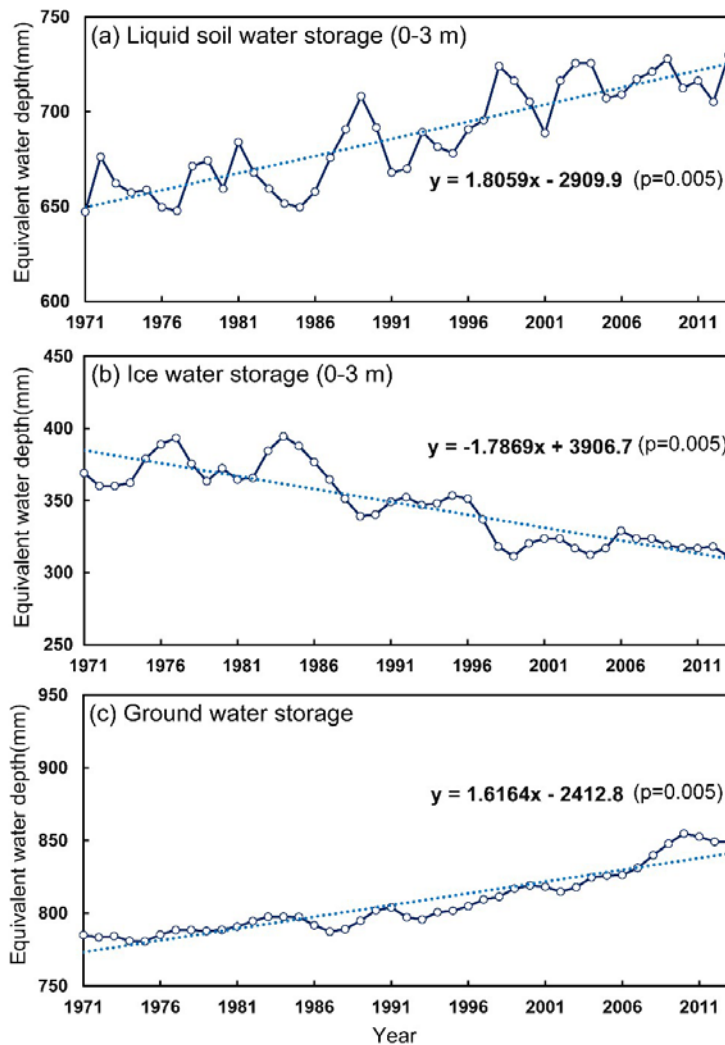
934 the thawing season. Trend lines are for simulated data. The upper two panels are for

935 freezing season and the lower two panels are for thawing season.

936

**Comment [PDM97]:** In order to better separate the two pairs of panels, I suggest moving the "(a) Freezing season" and "(b) Thawing season" titles outside of the panels. This will provide a bit of further separation between the pairs.

**Comment [PDM98]:** Data and regression results are shown. The upper



937

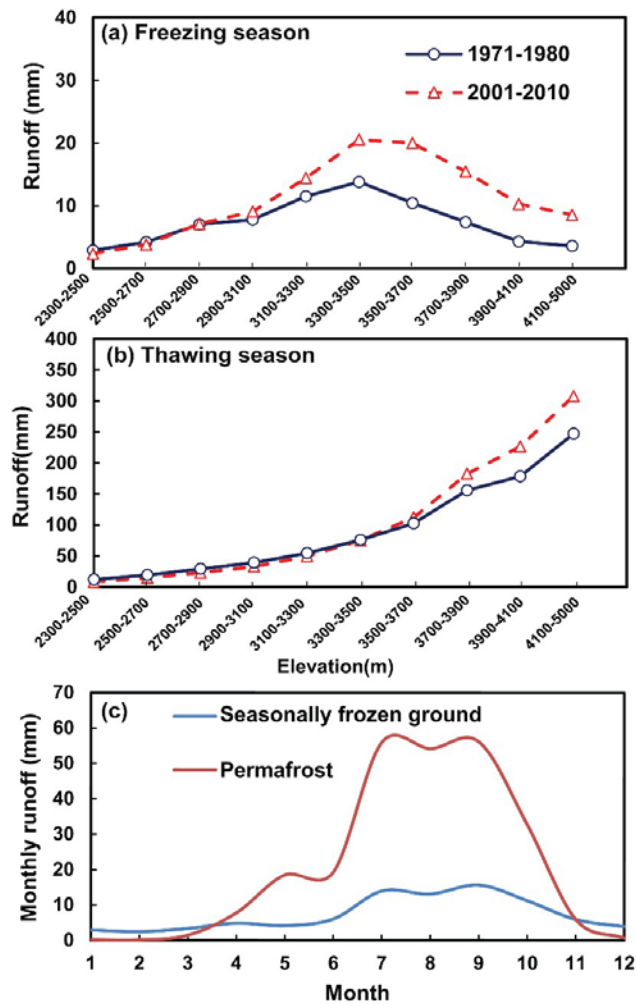
938 Figure 12. Basin averaged annual water storage (equivalent water depth) changes

939 simulated over the period of 1971 to 2013 for: (a) liquid water in the top layer of the

940 ground (0-3 m); (b) ice in the top layer of the ground (0-3 m); (c) and ground water.

**Comment [PDM99]:** You use "groundwater" in some places, and "ground water" in others. Please be consistent and make appropriate changes.

**Comment [PDM100]:** "water." Results from linear regressions are indicated."



941

942 Figure 13. Model simulated runoff changes from the 1971-1980 period to the 2001-  
 943 2010 period with elevation for (a) the freezing season and (b) the thawing season, and  
 944 (c) monthly averaged seasonal runoff in permafrost and seasonally frozen ground for  
 945 the period of 2001-2010.

946

947

948

949

Comment [PDM101]: "showing changes"

950 **Table list:**

951 Table 1 Major parameters of the GBEHM model.

952 Table 2 Changes in annual basin water balance and runoff components in different seasons.

953

954 Table 1 Major parameters of the GBEHM model

Comment [PDM102]: 1.

Parameters	Coniferous Forest	Shrub	Steppe	Alpine Meadow	Alpine Sparse Vegetation	Desert
Surface retention capacity (mm)	30.0	25.0	10.0	15.0	15.0	5.0
Surface roughness (Manning coefficient)	0.5	0.3	0.1	0.1	0.1	1.0
Soil reflectance to visible light	0.20	0.20	0.20	0.28	0.14	0.11
Soil reflectance to near-infrared radiation	0.225	0.225	0.225	0.28	0.225	0.225
Leaf reflectance to visible light	0.105	0.105	0.105	0.105	0.105	—
Leaf reflectance to near-infrared radiation	0.35	0.58	0.58	0.58	0.58	—
Leaf transmittance to visible light	0.05	0.07	0.07	0.07	0.07	—
Leaf transmittance to near-infrared radiation	0.10	0.25	0.25	0.25	0.25	—
Maximum Rubisco capacity of top leaf ( $10^{-5} \text{ mol} \cdot \text{m}^{-2} \cdot \text{s}^{-1}$ )	6.0	6.0	3.3	3.3	3.0	—
Plant root depth (m)	2.0	1.0	0.40	0.40	0.1	0.0
Intrinsic quantum efficiency ( $\text{mol} \cdot \text{mol}^{-1}$ )	0.08	0.08	0.05	0.05	0.05	—
Canopy top height (m)	9.0	1.9	0.3	0.3	0.2	—
Leaf length (m)	0.055	0.055	0.3	0.3	0.04	—
Leaf width (m)	0.001	0.001	0.005	0.005	0.001	—
Stem area index	0.08	0.08	0.05	0.05	0.08	—

955 Table 2 Changes in annual basin water balance and runoff components in different seasons

Comment [PDM103]: 2.

Decade	P (mm/yr)	E (mm/yr)	Sim R (mm/yr)	Obs R (mm/yr)	Runoff ratio (Obs)	Runoff ratio (Sim)	Runoff components (mm/yr)					
							Freezing season (from November to March)			Thawing season (from April to October)		
							T	G	S	T	G	S
1971-1980	439.1	282.1	154.1	143.8	0.33	0.35	18.5	0.0	0.0	135.6	3.5	13.8
1981-1990	492.8	300.8	188.5	174.1	0.35	0.38	20.5	0.0	0.0	168.0	3.1	27.8
1991-2000	471.0	307.6	161.9	157.4	0.33	0.34	20.5	0.0	0.0	141.4	3.8	18.4
2001-2010	504.3	319.0	180.6	174.3	0.35	0.36	26.2	0.0	0.0	154.3	3.7	24.1

Comment [PDM104]: "component ( $\text{mm} \cdot \text{y}^{-1}$ )". If you make this insertion, you can delete "(mm/yr)" from each of the column headers.

956 Note: P means precipitation, E means actual evaporation, R means runoff, T means total runoff, G  
 957 means glacier runoff and S means snowmelt runoff, Sim means simulation and Obs means  
 958 observation.